Spatially explicit negative prognosis of Cercospora leaf spot epidemics by process-based integration of leaf area index from remote sensing

Rene HJ Heim[1*], Paul Melloy[3**], Facundo Ramón Ispizua Yamati[2], Nathan Okole[2,4], Anne-Katrin Mahlein[2]

[1]University of Göttingen, Cartography, GIS and Remote Sensing, Goldschmidstr. 5, 37077 Göttingen, Lower Saxony, Germany

[2]Institute of Sugar Beet Research, Holtenser Landstraße 77, 37039 Goettingen, Lower Saxony, Germany

[3]CSIRO, Agriculture and Food, Dutton Park, 4102, Queensland, Australia

[4]Faculty of Agriculture and Environmental Sciences, Université Evangélique en Afrique, Bukavu 3323, Democratic Republic of the Congo

*Corresponding author: Rene HJ Heim, Email: rene.heim@uni-goettingen.de

** Rene HJ Heim and Paul Melloy contributed equally.

Funding

This work has partially been funded by the Deutsche Forschungsgemeinschaft (DFG, German Research Foundation) under Germany's Excellence Strategy, EXC-2070 - 390732324 – PhenoRob. This research was supported by funds of the Federal Ministry of Food and Agriculture (BMEL) based on a decision of the Parliament of the Federal Republic of Germany. The Federal Office for Agriculture and Food (BLE) provides coordinating support for artificial intelligence (AI) in agriculture as funding organisation, grant number FKZ 28DE104A18. Rene Heim was funded by the Deutsche Forschungsgemeinschaft (DFG, German Research Foundation) - 521313940.

Abstract

Crop production faces increasing constraints in managing biotic threats due to fungicide resistance, regulatory restrictions, and social pressures. While European farm chemical use requires justification, in-field spatial variability can lead to inaccurate assessments. We demonstrate the benefits of "episensing", linking remote sensing estimates of leaf area index (LAI) with a Cercospora leaf spot (CLS) epidemiological model for sugar beet (*Beta vulgaris*). We developed *cercospoRa*, an R package implementing a weather-based negative prognosis CLS model that requires canopy closure dates for initialization. We compared the conventional approach providing a single earliest estimated epidemic onset (EEEO) date for an entire field with an automated pixel-wise episensing workflow. To generate spatially explicit prognosis dates, we integrated a radiative transfer model with the CLS model, comparing uncrewed aerial systems (UAS) and Sentinel-2 (S2) imagery for estimating LAI and determining canopy closure dates. A General Additive Model confirmed that the *cercospoRa* package successfully performed negative prognosis 21 das (days after sowing) earlier $(\hat{\mu}_{\mathrm{UAS}} = 135.2\ \mathrm{das}, \mathrm{SE} = 1.3)$ than the observed epidemic onset $(\hat{\mu}_{\mathrm{observed}} = 156.9\ \mathrm{das}, \mathrm{SE} = 0.4)$. Spatial analysis revealed greater variability in predicted onset dates from higher resolution remote sensing products $(\mathrm{SD}_{\mathrm{UAS}} = 12.5)$ compared to low resolution products $(\mathrm{SD}_{\mathrm{S2}} = 8.8)$. These results demonstrate that an episensing approach provide higher precision and automation capacity to provide greater spatial context by applying models at the pixel level, revealing spatial variability that classic field-scale or regional prognosis cannot resolve. Future improvements should consider additional variables and inoculum pressure for more precise epidemic onset definitions, alongside development of spatially explicit reference data.

Keywords

canopy closure, episensing, FAIR, plant disease, sentinel 2, smart farming, uas

59

Introduction

Plant pathogens threaten global food security, with annual yield losses exceeding 30% in major crops despite intensive management efforts (Savary et al. 2019). Among these threats, *Cercospora beticola* (Dothideomycetes: Mycosphaerellaceae) stands as the most devastating foliar pathogen of sugar beet (*Beta vulgaris*), causing Cercospora leaf spot (CLS) epidemics that reduce recoverable sucrose yields by up to 50% under favorable conditions (Rangel et al. 2020; Shane and Teng 1992). This hemibiotrophic fungus employs a polycyclic disease cycle, producing 100–300 conidia per lesion every 7–10 days under optimal temperatures (25–30°C) and humidity (Rangel et al. 2020), enabling rapid epidemic development that challenges conventional control strategies. Modern CLS management relies on an integrated framework combining 3-year crop rotations, partial host resistance cultivars, and targeted fungicide applications (Barreto et al. 2023; Spanner et al. 2022). However, the pathogen's genetic plasticity has accelerated resistance evolution to all major fungicide classes – including benzimidazoles, quinone outside inhibitors, and demethylation inhibitors – with resistant strains now reported across European and North American production regions (Rangel et al. 2020; Spanner et al. 2022). Still, Germany maintains its position as Europe's leading sugar beet producer, with 31.6 million tonnes harvested in 2023 representing 28.6% of total EU production (Eurostat 2023). To maintain this productivity and to assist judicious fungicide applications, mechanistic and empirical forecasting models have been developed to improve spray efficiency (El Jarroudi et al. 2021; Racca and Jörg 2007; Wolf and Verreet 2005).

Recent syntheses of plant disease modeling paradigms emphasize the transformative potential of sensor networks and automated data pipelines in managing polycyclic pathogens like *C. beticola*. Contemporary approaches bifurcate into data-driven empirical models and process-based mechanistic frameworks, each addressing

distinct aspects of CLS epidemiology (Skelsey 2021; González-Domínguez et al. 2023; Mahlein et al. 2024). Empirical models are commonly grounded on the analysis of past and present meteorological data to predict future disease outbreaks (Shah et al. 2019). Mechanistic models attempt to simulate disease development based on an understanding of the biological processes and describe disease infection, latent periods, reproduction and spread mathematically (Chaloner et al. 2019). Most research, as described by González-Domínguez et al. (2023), complements the mechanistic approach by exploring the dynamics of the host, pathogen, and environment within the pathosystem, defining condition limits and optimums based on limited data. Theoretically, this approach enables greater spatiotemporal transferability, as it is inherently driven by environmental variables. However, it is sometimes constrained by the lack of information about the inoculum source, quantity, and spatial distribution. In contrast, the data-driven empirical approach, also outlined by González-Domínguez et al. (2023), typically regresses pathosystem variables with restricted spatiotemporal predictors, which may lack direct biological relevance to the epidemic. Thus, empirical models can define parameter variation and are not limited by a defined mechanistic relationship. With sufficient data quality and quantity to characterize all potential pathogenic states of the pathosystem, empirical models can provide satisfying results with careful predictor selection. Inference from empirical studies are also valuable for exploratory studies looking for new mechanistic links. Both types of models require validation through field trials before they can be used when forecasting epidemics. Inherently, plant disease modelling grapple with numerous possible unknown spatial parameters representing distributions of host genotypes, different pathogen strains and microclimates beyond a single species at a single location (Cunniffe et al. 2015; Garrett et al. 2018).

Remote sensing of vegetation (i.e., collecting non-contact sensor data of plant canopies) has revolutionized our understanding of ecosystems and managed landscapes by revealing spatial patterns at multiple geographical scales (Jones and Vaughan 2010). Another key advantage of remote sensing is its ability to monitor biochemical and structural vegetation traits and functions (Asner 1998), which are crucial for understanding how natural and managed landscapes adapt to environmental changes such as biotic and abiotic stress (Jackson 1986). Structural plant traits and their developmental stages can be remotely monitored using sensing techniques, providing important predictors of plant disease epidemiology (Guan and Nutter 2002; Homolová et al. 2013; West et al. 2003). The strengths of remote sensing have been exploited for detecting the presence, incidence, and severity of diseases (Barreto et al. 2023; Bock et al. 2020; Heim et al. 2019; Kuska et al. 2022; Mahlein et al. 2024). However, leveraging remote sensing for mechanistic, epidemiological disease modelling and the exploration of spatial disease patterns is under-represented in the literature. Given the complex heterogeneous edaphic, environmental and microclimate conditions in time and space that control presence and intensity of plant disease (Cunniffe et al. 2015), remote sensing seems a suitable tool to be integrated into epidemiological modelling workflows as it allows to capture biochemical and structural field-scale and landscape patterns of host and pathogen alike (Berger et al. 2022; Ojiambo et al. 2017). The suitability of remote sensing to be integrated into plant epidemiology has now been validated with the coining of the term “episensing”, the use of remote sensing data and sensor networks to inform and enhance epidemiological models of plant disease, enabling more precise surveillance, risk assessment, and management of plant health (Mikaberidze et al. 2025).

In Germany, fungicide application decisions for CLS are guided by a threshold system based on disease incidence (DI; Wolf and Verreet 2002). DI is assessed by regional

plant protection and advisory services but must also be confirmed by growers at their local fields. This requires growers to count the number of leaves within their field with at least one characteristic CLS lesion from 100 randomly sampled leaves. If DI reaches 5% before August 15, the potential yield losses are estimated as unacceptable, prompting the first fungicide application. To keep optimizing CLS management and yield, the mechanistic rules for CLS epidemics in sugar beet have partially been elucidated and it was shown that they are predominantly influenced by environmental conditions, specifically, temperatures above 15°C and relative humidity exceeding 60% (Vereijssen et al. 2007). The dissemination of conidia to the abaxial surfaces of leaves or petioles, facilitating infection, occurs via wind, rain, irrigation, water splash, or insect vectors. Optimal conditions for the germination of conidia include near-saturated relative humidity and temperatures around 25°C (Khan et al. 2007). To reliably start the sampling at local fields, timing of epidemic onset must be predicted but this has been found to be highly variably across sites and seasons (Wolf and Verreet 2005). A series of infection trials by Wolf and Verreet (2005) highlighted that the commencement of problematic epidemics could occur anytime from early July to mid-September. Their goal was to determine the origin of this variation to optimize the prediction of epidemic onset. The sources of variability were partly explained by different susceptibility levels of cultivars and the timing of canopy closure, the later of which results in a more disease-conducive micro-climate. Additionally, weather-related factors were explored as possible explanations for the differences in the timing of epidemic onset. They concluded that high variations are a barrier for predicting epidemic onset to a single date and making accurate management decisions. However, they found a negative prognosis assessing the most likely periods of disease absence was possible, reducing disease surveillance requirements early in the season (Wolf and Verreet 2005). Other efforts to improve the accuracy for estimating fungicide intervention thresholds have

concentrated on refining relative humidity thresholds (Khan et al. 2007), exploring optimal model start times and cultivar susceptibility for CLS negative prognosis models which rely on cumulative daily infection values (cDIV) (Wolf and Verreet 2005). Commercial models, such as, CERCBET1 and 3(+), primarily utilize parameters such as temperature, relative humidity, leaf wetness, vapor pressure deficit, cultivar susceptibility, and disease incidence (Racca and Jörg 2007). Some manuscripts have argued to improve accuracy for modelling the complex dynamics of CLS epidemiology by gaining a comprehensive understanding of spatiotemporal dispersal mechanism of *C. beticola* spores (Imbusch et al. 2021) and canopy cover (Wolf and Verreet 2005). However, spatial heterogeneity of CLS has not been investigated but is a relevant factor to understand when pathogens are dispersed by wind as is the case for *C. beticola*. When in-field variability is large, current transect-based assessments extremely might be inappropriate for correctly determining fungicide intervention thresholds for CLS.

As the spatial variability of structural plant parameters such as canopy cover is difficult to measure directly without extensive manual field sampling, it is possible to obtain estimates using the leaf area index (LAI) as a proxy. LAI can be retrieved through the inversion of radiative transfer models (Fang et al. 2003). Several studies have achieved reasonable estimations of leaf and canopy chlorophyll contents and LAI using RTMs in row crops (Dorigo 2012; Duan et al. 2014) and also in sugar beet trials (Andrieu et al. 1997; Jay et al. 2017). As LAI is the total one-sided leaf area per ground area, and an indicator of the canopy's ability to photosynthesize and intercept light, it is a fundamental driver of the relationship between spectral signal intensity, spectral shape, and canopy characteristics (Curran and Milton 1983). In sugar beet, and other species such as corn (*Zea mays*) or winter wheat (*Triticum aestivum*), LAI shows a direct relationship with canopy cover (Nielsen et al. 2012; Tillier et al. 2023) and therefore

189 can be used as a proxy for canopy closure. Spatial variations in LAI are driven by leaf
190 area and leaf angle (Fang et al. 2019; Zou et al. 2018). Further, the availability of soil
191 water, soil compaction and other edaphic factors can result in phenotypic differences
192 of sugar beet plants that as well can be reflected in spatial variability of LAI (Garrigues
193 et al. 2008; Saiz-Rubio and Rovira-Más 2020; Tittonell et al. 2013). Canopy density
194 and closure define the infestation of crop pests and diseases by modifying the humidity
195 and temperature fluxes, therefore creating differently suitable microclimates for pest
196 and disease development (Faye et al. 2017; Pielaat et al. 2002; Vidal et al. 2017).

197 This study addresses two critical limitations in CLS epidemiological modeling: (1)
198 restricted accessibility of validated forecasting tools, and (2) spatial homogeneity
199 assumptions in regional-scale models. We advance CLS management through two
200 integrated objectives:

201 1. Open-source epidemiological framework

202 We aim at operationalizing Wolf and Verreet's negative prognosis model (Wolf and
203 Verreet 2005) as the R package *cercospoRa*, implementing their infection rules for
204 hourly temperature and moisture effects while adhering to FAIR principles.

205 2. Pixel-level negative prognosis for CLS

206 Traditional regional models assume uniform canopy development. As Wolf and Verreet
207 (2005) emphasize the importance of canopy closure as a critical phenological event
208 for initiating their negative prognosis model, we saw the opportunity to harness
209 airborne and spaceborne multispectral remote sensing imagery to obtain spatially
210 explicit (i.e., pixel-wise) canopy closure timing by linking LAI maps with canopy cover
211 dates. This we used to reveal spatial variability of the earliest estimated epidemic onset

on a sub-paddock scale, thereby improving modeling results in comparison to field scale approaches.

In summary, this research addresses the growing need for adherence to FAIR (Findable, Accessible, Interoperable, and Reusable) principles in epidemiological research and responds to calls for methods that allow studying the spatial dynamics of epiphytotics (Cunniffe et al. 2015; Grünwald et al. 2024; Mikaberidze et al. 2025; Morris et al. 2022; Sparks et al. 2023).

Methods

CercospoRa Package

The *cercospoRa* R package was developed by translating CLS epidemiological formulas from prominent CLS models published in academic journals (Wolf and Verreet (2005), El Jarroudi et al. (2021), and Racca and Jörg (2007). The model described by Wolf and Verreet (2005) provided the most reproducible methods and therefore was chosen as the primary model to test with remote sensing data. Basic functionality and descriptions of the package structure and functions are provided in the supplementary information (S1 – S5). The current stable version of the package (1.0) requires (R ≥ 4.3.0) and is available on via the Comprehensive R Archive Network (CRAN). A development version of the package is available on Github (https://github.com/PaulMelloy/cercospoRa/tree/dev). The package builds on the published methods of Wolf and Verreet (2005) with the aim of supporting an automated workflow.

To generate the following results, daily Infection Values (DIV) were summed (cDIV) and associated to variety ranking system (see S7) based on the published data in Wolf Verreet (2005).

$$cDIV_{thres} = 12.4724 - S * 4.6431 \quad \textit{Equation 1}$$

Where '$cDIV_{thres'}$ is the cumulative Daily Infection Values threshold for the earliest estimated epidemic onset date as determined by negative prognosis model. '*S'* is the susceptibility coefficient, was calculated by the following equation:

$$When\ V\ \geq 4\ \Rightarrow S = \sqrt{V-4} \qquad \textit{Equation 2}$$

$$When\ V\ < 4\ \Rightarrow S = -\sqrt{4-V} \qquad \textit{Equation 3}$$

Where V is the varietal susceptibility value (e.g. 6 for our variety) from the scale described in the guidelines for conducting agricultural value tests and variety trials provided publicly by the Federal Plant Variety Office (Bundessortenamt 2000). Susceptibility ratings are done on a yearly basis and updated in the Descriptive Variety Lists (Bundessortenamt 2022). Additional functions are incorporated in the package to allow the use of remote sensing imagery for calculating canopy closure dates and translating these dates into negative prognosis dates for epidemic onset.

Experimental Trial

In 2022, a field trial was conducted on a clay loam soil near Göttingen, Germany (Latitude: 51.498, Longitude: 9.916), to analyze disease dynamics of CLS, caused by *Cercospora beticola*, in sugar beet (*Beta vulgaris*). The susceptible (medium to strong = 6) sugar beet cultivar Aluco (SESVanderHave, Tienen, Belgium) was sown on 2022-03-31, with an inter-row distance of 48 cm, an intra-row distance of 18 cm, and an expected seeding rate of approximately 110,000 plants per hectare. The total area covered 1.25 hectares. According to the Köppen-Geiger climate classification (Beck et al. 2018), the region has a temperate continental climate with high-temperature ranges between summer and winter, with temperatures routinely falling below freezing in winter (i.e., Dfb - Continental). The site has a long-term average temperature of 8.7 °C,

an approximate elevation of 150 m, and 645 mm in average annual precipitation. A regional weather station (DALOS 515-WD, F&C GmbH, Germany) was used for continuous measurements of relative humidity (RH) and air temperature (T). These meteorological data was used to fit the *cercospoRa* model (Supp. Information Eq. 1-6) and is provided along with the *cercospoRa* package.

The sugar beet trial (Figure 1 A-D) was inoculated in a radius of 10 m with *C. beticola* (Figure 1 A-C, white dashed-line circle). Inoculation was applied on 2022-04-11 using CLS-affected sugar beet plant material, which was obtained by drying identical sugar beet cultivars from the previous year, as described by Imbusch et al. (2021). Sampling for data analysis was done across two levels, for the inoculation area itself with an additional buffer of 10 m (Figure 1 A-C, white solid-line circle) and for the remaining area excluding the inoculation area (Figure 1 A-C, white dashed-line frame).

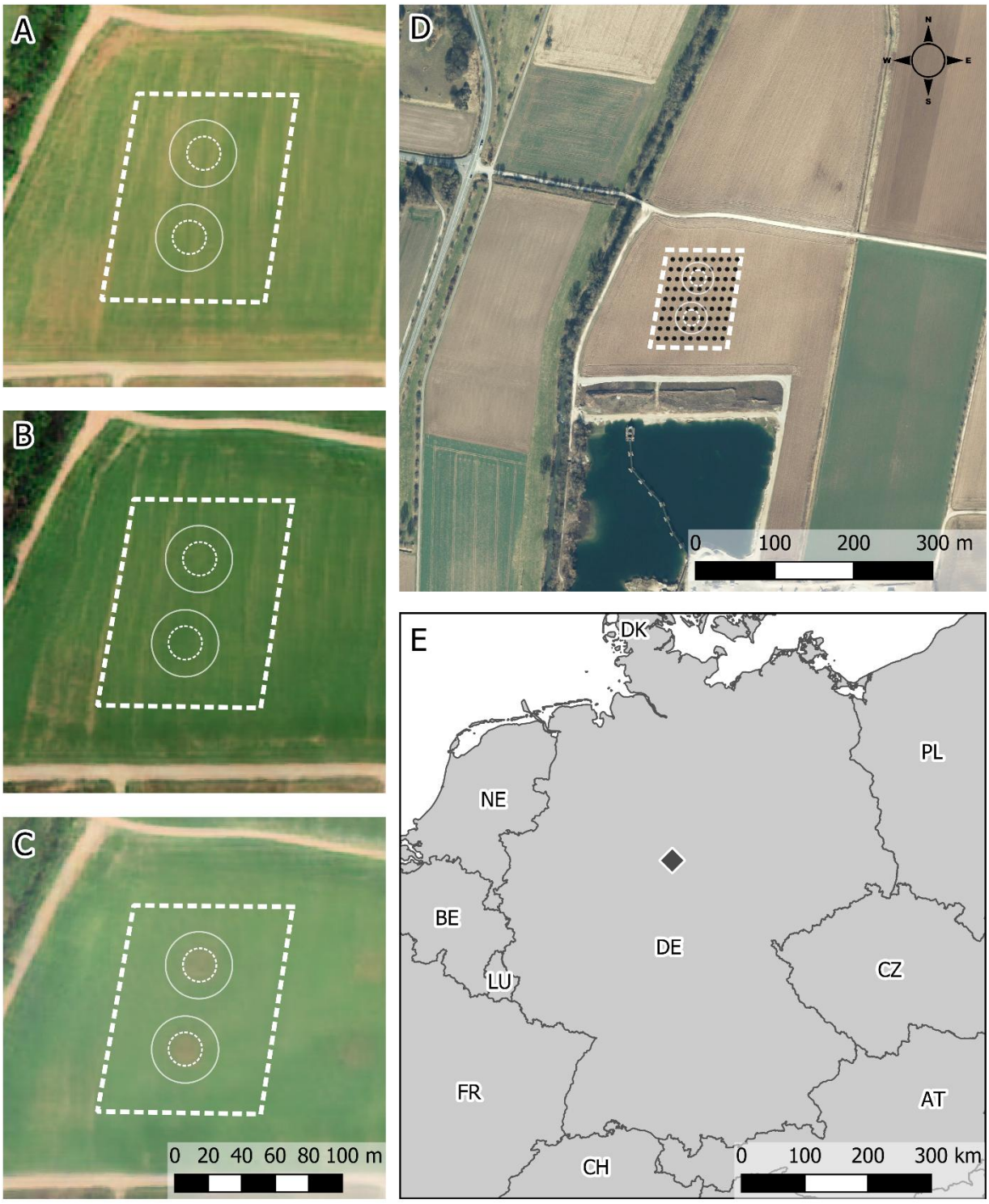


Figure 1. *Experimental sugar beet trial close to Göttingen, Germany (E, black diamond shape). Map A-C display the site in June, July and early September 2022. Solid white circles (A - D) indicate the sampling zone (radius = 20 m) of the inoculated area (dashed line, radius = 10 m). The remaining and larger area (rectangular dashed-line frame) was sampled as non-inoculated area. Between sowing and harvest, sparse disease severity sampling was done on 5-15 plants within the systematically placed circular, black areas (D).*

Plant Disease Data

To validate the CLS model by Wolf and Verreet (2005), it was necessary to obtain pixel-wise (i.e., dense) disease scoring data. This data was generated based on sparse manual sampling. Sparse plant-level disease severity (DS) scores were collected from sowing (2022-03-31) to harvest (September 2022) through nearly weekly manual evaluations, which were intentionally synchronized with UAS flight days to ensure temporal consistency. More than 200 geospatially distributed field locations were surveyed, with approximately 20 plants assessed per location following the scale and methodology described by Günder et al. (2025), using RTK for precise geolocation. This scale defined healthy plants at a score of ‘one’ and a plant with at least one CLS lesion as ‘two’. Wolf and Verreet (2005), defined ‘epidemic onset’ as the stage at which at least 50% of the plants exhibit a minimum of one CLS lesion (corresponding to 0.01% diseased leaf area). Therefore, for each assessment location in this trial we defined epidemic onset when at least 50% of plants were scored as diseased (two or greater based on severity).

Remote Sensing Data

Throughout the vegetative period a quadrocopter DJI Matrice 210 RTK V2 (DJI Technology Co., Ltd., Shenzhen, China) was used as a camera platform. The position of the UAS during the flight was determined by GPS and GLONASS and corrected by the D-RTK 2 Mobile Station (DJI Technology Co., Ltd., Shenzhen, China). A mounted Micasense Altum multispectral camera (AgEagle Aerial Systems Inc., Kansas, USA) captured six bands and carried a Downwelling Light Sensor V2 (AgEagle Aerial Systems Inc., Kansas, USA). The bands had the following specifications: blue (475 nm center, 32 nm bandwidth), green (560 nm center, 27 nm bandwidth), red (668 nm center, 14 nm bandwidth), red edge (717 nm center, 12 nm bandwidth), near infrared (842 nm center, 57 nm bandwidth), and long-wave thermal infrared (8000-14000 nm).

The long-wave thermal infrared was not used in the radiative transfer modelling (RTM) inversion process.

The effective ground sampling distance was 9.5 mm at an altitude of 22 m above ground level. Horizontal and vertical overlap were set to 75 %. These settings allowed a speed of 3 m/s. The entire field was covered in three consecutive flights. Multispectral images were post-processed and radiometrically calibrated using a standard calibrated reflectance panel (AgEagle Aerial Systems Inc., Kansas, USA) with known reflectance values across the entire measured spectrum (250nm to 950nm), using Metashape (Agisoft LLC, St. Petersburg, Russia).

Sentinel-2 (S2), level-2A, multispectral images (e.g., Drusch et al. 2012) with a spatial resolution of 10 m obtained from the European Space Agency's Copernicus Data Space Ecosystem which was accessed on 2024-03-01. The level-2A data is already atmospherically corrected and provides surface reflectance values, derived from the associated Level-1C products. Each level-2A product is composed of 110 x110 km^2 tiles in cartographic geometry (UTM/WGS84 projection). The S2 images were acquired for the same weeks as when UAS data was collected and selected with a cloud cover of less than 30%, ensuring high quality data for the analysis. To prepare the data for RTM, individual bands were stacked into a single raster file. These bands were chosen to allow comparability with the UAS-mounted multispectral camera and included Band 2 (blue: 490 nm, 10 m resolution), Band 3 (green: 560 nm, 10 m resolution), Band 4 (red: 665 nm, 10 m resolution), Band 5 (red edge: 705 nm, 20 m resolution), and Band 8 (near infrared: 842 nm, 10 m resolution).

Super-Resolution

To further enhance spatial detail in our analysis, we applied the S2DR3T single-image super-resolution model, a deep learning framework specifically optimized for Sentinel-

2 Level-2A multispectral data (Akhtman 2025). Super-resolution refers to a suite of computational and optical techniques designed to enhance the spatial resolution of images beyond the inherent limitations of the original imaging system. S2DR3T is used to upscale native resolution (10 m, 20 m, and 60 m) Sentinel-2 imagery to a refined 1-meter resolution, while promising to preserve subtle spectral signatures in both soil and vegetation across all bands. This approach effectively bridges the spatial gap between UAS and native resolution satellite data, improving the interpretability and precision of pixel-level LAI and canopy closure mapping. The resulting high-resolution products (S2S) support more detailed and scalable spatial disease risk modeling and demonstrate the potential of super-resolution techniques for future developments in precision agriculture and plant disease epidemiology.

Generating LAI Maps

The *cercospoRa* package estimates the epidemic onset through the timing of sugar beet canopy closure. PRO4SAIL was implemented via the R package hsdar (Meyer and Lehnert 2022) which combines the leaf-level RTM PROSPECT 5b (Feret et al. 2008) and the canopy-level RTM 4SAIL (Verhoef et al. 2007). PRO4SAIL has been successfully used to retrieve LAI in sugar beet, achieving an RMSE below 10% (Berger et al. 2018; Jay et al. 2017). However, caution is required when applying PRO4SAIL to row crops, as it was originally designed for homogeneous, horizontally uniform canopies. For broad, glossy leaves such as those of sugar beet, reflectance data collected from within the sun hotspot and a high specular component can lead to retrieval inaccuracies (Andrieu et al. 1997). Recent studies confirm that PRO4SAIL can be effectively applied to row crops when fractional cover is high (Han et al. 2023), as observed in later growth stages, consistent with our study.

PROSPECT 5b simulates the leaf directional hemispherical reflectance and transmittance from 400 to 2500 nm as a function of leaf biochemistry and internal

structure. PROSPECT 5b (PS) parameters are N[1], C_{ab}[2], C_{ar}[3], C_{br}[4], C_w[5], and Cm[6]. The canopy-level RTM 4SAIL (4S) is used to simulate the bidirectional reflectance factor (Schaepman-Strub et al. 2006) of turbid medium plant canopies, by solving the scattering and absorption of two direct fluxes (i.e., incident solar flux and radiance in the viewing direction) and two diffuse fluxes (i.e., upward/downward hemispherical flux). The bidirectional reflectance factor is described by key plant parameters such as the LAI[7], the canopy type described as lidf[8], hspot[9], and soil[10]. Other relevant parameters are those describing the sun-sensor geometry; θ_{rel}[11], φ_{sun}[12], and φ_{obs}[13]. In forward mode, RTMs convert plant parameters into reflectance spectra. Initially, a look-up table is created that contains a range of reflectance spectra generated based on the RTM parameters (Table 1). To find the best reflectance spectra matches between the database and the spectra that were collected, the PRO4SAIL spectra had to be resampled to resemble the wavelength and band centers of the Altum multispectral camera used in this study. Then the spectral angle mapper (SAM) algorithm (Kruse et al. 1993) was applied to minimize the error (i.e., maximize the cosine of the angle) between modelled and measured multispectral signatures. Various studies have used the RMSE as a loss metric, however during model optimization, it was found that the SAM algorithm outperformed the RMSE in this study. The inversion for LAI retrieval was parameterized using the minimal necessary, but realistic, value ranges to reduce computational effort. Modelled LAI values were compared to empirical data of previous

[1] leaf structure parameter [unitless]
[2] chlorophyll a + b content [µg*cm^{-2}]
[3] carotenoid content [µg*cm^{-2}]
[4] brown pigment content [unitless]
[5] equivalent water thickness [cm]
[6] leaf mass per area [g*cm^{-2}]
[7] Leaf area index [m^2 * m^{-2}]
[8] leaf inclination distribution function [unitless]
[9] hot spot parameter [unitless]
[10] soil brightness [unitless]
[11] relative azimuth angle [°]
[12] sun zenith angle [°]
[13] observer zenith angle [°]

studies (Hoffmann and Blomberg 2004; Tillier et al. 2023). These studies reported that LAI rarely exceeded LAI values of 6, therefore we limited the inversion of PRO4SAIL to the LAI range of 0-6. The remaining parameter ranges have been selected based on typical parameters for the evaluated growing stage (Jay et al., 2018).

TABLE 1 HERE

Generate Pixel-Wise LAI Progression Curve

Spatial variability in LAI, and therefore canopy cover, can cause local micro-climate differences, and cause spatial variability of pests and diseases (Faye et al. 2017). The negative prognosis model by Wolf and Verreet (2005) commences at canopy closure (i.e., when leaves from 90% of plants in adjacent rows have their leaves touching). As the spatial variability of canopy closure at field-scale is difficult to observe from the ground but can be visualized by the pixel-wise retrieval of LAI based on multispectral satellite and UAS images in combination with RTMs, we implemented RTM-based retrieval of LAI as a useful tool to enhance classic disease modelling by automating and standardizing the monitoring for canopy closure date. Three LAI maps, one for each remote sensing platform (UAS, S2, and S2S) were derived from images acquired well in advance to the expected epidemic onset. UAS imagery was collected on June 14 and June 28, 2022, while Sentinel-2 (S2, S2S) imagery was acquired on June 10 and June 30, 2022, resulting in a ~20-day monitoring window for both platforms. The full workflow is provided below (Figure 2)

As the canopy closure date cannot be known in advance, we developed a sigmoidal function (Eq. 4) modelling the evolution of LAI over time for each pixel individually. Previous literature showed that the relationship between canopy cover and time approximates a sigmoidal function (Günder et al. 2022). Because of the close

relationship with LAI, the sigmoidal function was used to model growth curves (Figure 2, Box 3) for each pixel.

The fitted model is used to estimate the time at which a defined LAI threshold is reached, indicating the date of canopy closure (Eq. 5).

$$LAI = \frac{K}{1 + \left(\frac{K - LAI_0}{LAI_0}\right) * e^{-r*(t-t_0)}} \quad \textit{Equation 4}$$

Where K = the carrying capacity parameter (here: K = 6, close to maximum), a cultivar-dependent parameter representing the maximum LAI which can be attained, r = the growth rate parameter of sugar beet LAI, LAI_0 = the initial LAI value, and t_0 = the initial date.

To obtain the shape parameters (LAI_0 and r) for the sigmoidal function, at least two georeferenced LAI images of a location was needed. In this study we used radiative transfer modelling as the mechanistic link between plant parameters and LAI is well established. However, any other method to reliably obtain spatially resolved LAI values would be valid. For each pixel the shape parameters (LAI_0 and r) were estimated to minimize the squared error between measured LAI (i.e., obtained in the images) and modelled LAI (i.e., obtained from the fitted sigmoidal function). Based on the estimated shape parameters and the cultivar-dependent LAI threshold for canopy closure the actual date for canopy closure (t_{cc}) was calculated for each individual pixel (Eq. 5). LAI observations reported from earlier studies (Tillier et al. 2023) led to the selected LAI value 1.3 for canopy closure (i.e., 90% of row closure).

$$t_{cc} = t_0 + \frac{log\frac{LAI_{thresh} * (K - LAI_0)}{LAI_0 * (K - LAI_{thresh})}}{r} \quad \textit{Equation 5}$$

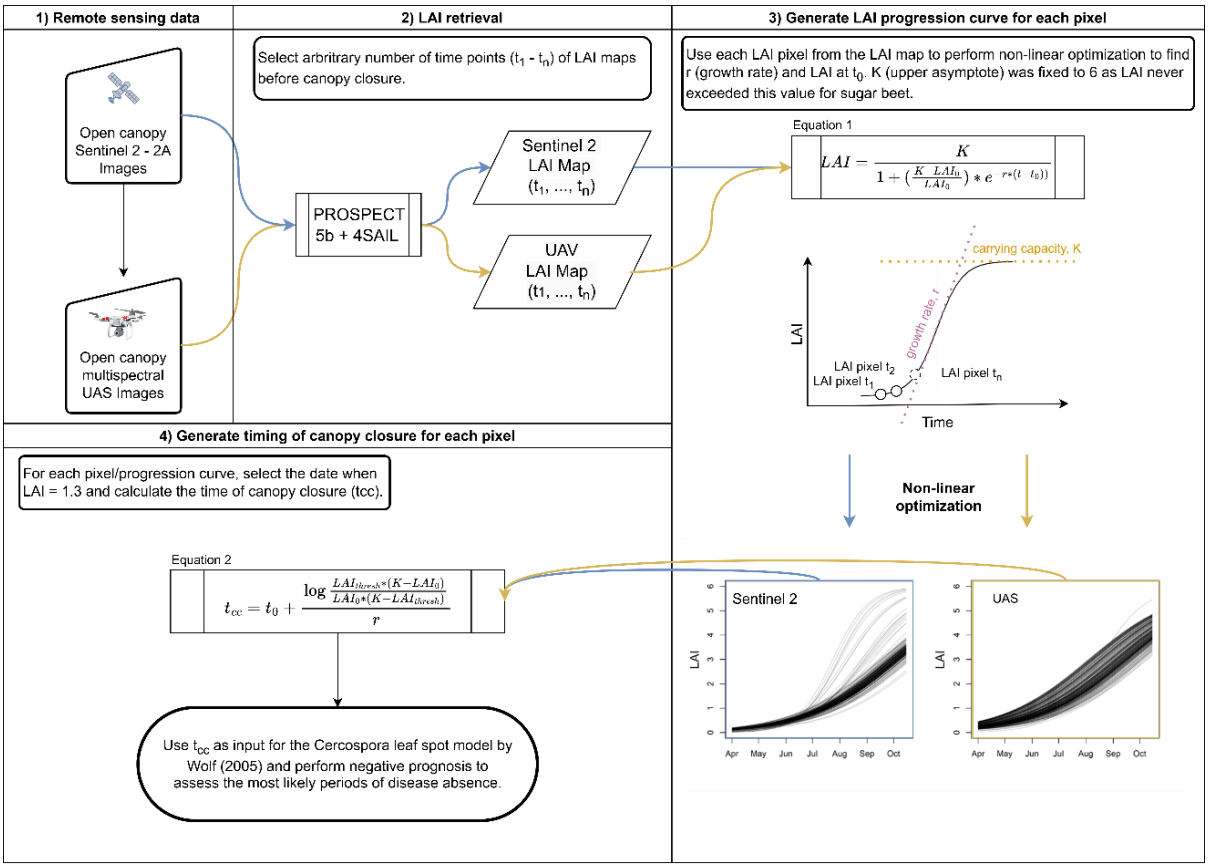


Figure 2. *Our workflow to allow pixel-wise negative prognosis of Cercospora leaf spot. We obtained airborne and spaceborne multispectral remote sensing data (1) which was used to retrieve pixel-wise leaf area index (LAI) values using radiative transfer modelling (2). At least two LAI maps, but more are possible, are needed to run our non-linear optimization that is based on a sigmoidal function (3). This process results in time-resolved LAI progression curves, also for each pixel. Eventually, each LAI progression curve can be used to obtain the timing of canopy closure depending on a cultivar-specific LAI threshold. The timing of canopy closure is used to start pixel-wise negative CLS prognosis based on the Cercospora leaf spot model by Wolf and Verreet (2005) as it was implemented in our cercospoRa R package.*

Analysis

Negative prognosis models incorporate the cumulative weight of weather conditions and predict when the disease has not yet established, or when it can't be certain that disease has not established (Ullrich and Schrödter 1966). The Wolf and Vereet (2005) CLS model provides a threshold date when epidemic onset is not likely to occur before, therefore correlative analyses with epidemic onset dates were not appropriate for this study. Canopy closure observed epidemic onset (EO) and earliest estimated epidemic onset (EEEO) days after sowing were analysed with a general additive model (GAM) from the mcgv R package (Wood 2017). Dependent variables, latitude and longitude

were fit as a basis spline to capture spatial variation attributed to soil and field gradients. Observation source, either visual by a skilled technician, UAS, S2, or S2S were tested as independent variables and with interaction if the observation was in inoculated field area.

Results

LAI Retrieval

Leaf Area Index (LAI) values varied between inoculated and non-inoculated areas (Table 2), remote sensing platforms, and acquisition dates. UAS based LAI retrieval consistently captured higher and more variable LAI values than Sentinel-2 retrieval (S2). Higher resolution, 0.31 m x 0.27 m, returned more detailed field features, such as wheel tracks and row spacing, compared with 10 m x 10 m resolution provided by S2.

S2 imagery showed stable LAI means of 0.5 m^2/m^2 at both time points in the inoculated area and low variability (SD: 0.07). In contrast, UAS data resulted in higher mean LAI values, 0.7 m^2/m^2 on 2022-06-14 and 0.72 m^2/m^2 on 2022-06-28, with greater variability (SD: 0.2).

LAI showed A similar trend in the non-inoculated areas. S2 derived LAI remained consistent with a mean 0.5 m^2/m^2 (SD: 0.08), while UAS-based estimates returned notably higher mean LAI estimates 0.7 m^2/m^2 (SD: 0.2) and 0.7 m^2/m^2 for time points, 2022-06-10 and 2022-06-30 respectively. The highest variability was again observed in the earlier UAS observation on 2022-06-10 (SD: 0.2; range: 0.3–1.5 m^2/m^2).

LAI retrieved from the Sentinel-2 super-resolution (S2S) product, having a resolution of 1 m x 1 m, showed values between those of the other products (i.e., S2 and UAS), in both, inoculated and non-inoculated areas. S2S-derived LAI remained stable across

observation dates (mean: 0.6 m²/m² and 0.6 m²/m², respectively), with moderate variability (SD: 0.1) (Table 2). S2S showed improved sensitivity compared with standard S2 while avoiding the higher variability seen in UAS data.

TABLE 2 HERE

Canopy Closure

Canopy closure date maps (Figure 3) were generated based on LAI maps. Since LAI maps were initially produced at the native spatial resolutions of the various image sources, the influence of spatial resolution was already accounted for. As a result, maintaining high resolution in the subsequent canopy closure mapping step was unnecessary, allowing for reduced computational demands. Therefore, the LAI maps from both UAS and S2S sources were downscaled to match the spatial resolution of Sentinel-2 imagery (10 m × 10 m), which was then used to produce the final canopy closure maps.

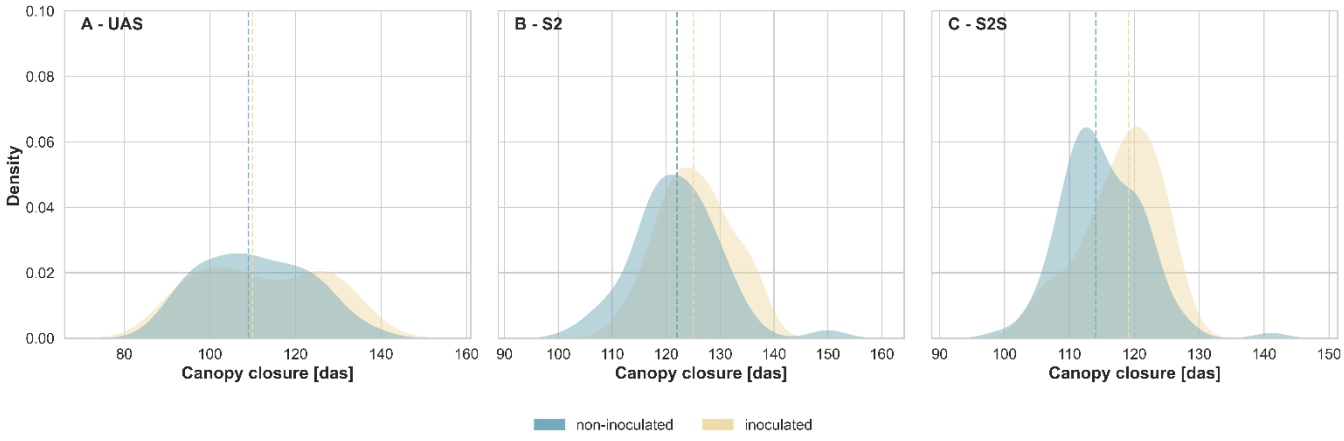


Figure 3. *Estimated canopy closure density distributions in 'days after sowing' (das) for the inoculated (linen white) and non-inoculated (soft blue) areas for each remote sensing platforms. (A) Unmanned aerial system, UAS; (B) Sentinal-2, S2; and (C) Sentinal-2 super-resolution S2S. Vertical dashed lines represent the medians for the respective inoculated treatments.*

TABLE 3 HERE

Based on visual assessment, canopy closure at the whole-field level occurred on 2022-07-30 (121 das). Remote sensing platforms with higher spatial resolution (i.e., S2S and

UAS) estimated significantly earlier mean canopy closure dates (Table 3 & 4). This earlier canopy closure trend between RS platforms was no different between inoculated and non-inoculated areas, indicating no interaction (P = 0.266). The General Additive Model (GAM) results support the trends observed in the canopy closure raw data (Table 3 & 4). Canopy closure occurs significantly earlier by a mean of 4.17 days in non-inoculated areas compared to inoculated areas (P = 0.001) regardless of the remote sensing platform. Sentinel-2, which had the lowest original spatial resolution (see LAI retrieval section), estimated an average canopy closure for non-inoculated areas at 121.6 das. S2S and UAS methods estimated canopy closure 6.9 days and 11.3 days earlier than S2 respectively (Table 4).

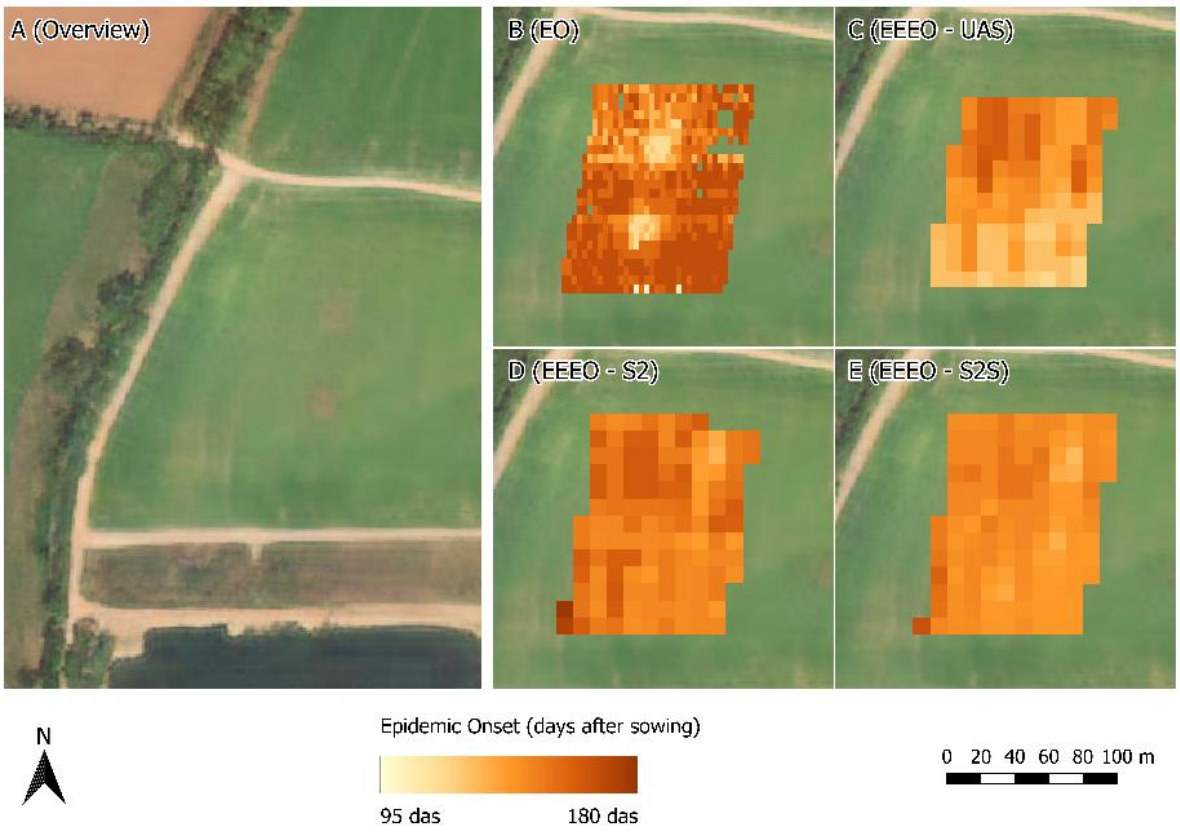
TABLE 4 HERE

Observed and earliest estimated epidemic onset

Canopy closure dates were parsed to the CLS negative prognosis model *cercospoRa*, which returned the estimated dates when the absence of CLS was no longer likely given the weather conditions and hence the earliest estimated CLS epidemic onset date (EEEO). Canopy closure was visually estimated as 2022-07-30 for the whole field which provided an EEEO date of 2022-08-19 (141 das).

TABLE 5 HERE

Visual inspection of EO within the field, in the non-inoculated region, ranged between 2022-07-06 (97 das) and 2022-09-14 (167 das) (Table 5) with a mean field EO date 2022-09-04 (157 das) (Table 6). EEEO from remote sensing platforms, S2, S2S and UAS, all showed significantly earlier mean EEEO dates by 10.34, 17.85 and 21.74 days compared to EO ($P < 0.001$) in the non-inoculated region (Table 6). EO in the inoculated areas ranged between 2022-07-20 (111 das) and 2022-09-14 (167 das), and a mean EO which was significantly earlier by 16 days compared to EO in non-inoculated areas ($P < 0.001$). Mean EEEO dates from remote sensing platforms S2, S2S in the inoculated areas however were later compared with the EO by 9.6 and 1.3 days respectively. Only high resolution UAS data resulted in slightly earlier EEEO values, by 2.6 days compared to EO in the inoculated areas. Observed EO and UAS data resulted in higher variation in both the inoculation and non-inoculation areas compared to S2 and S2S data (Table 5, Figure 4 and 5).

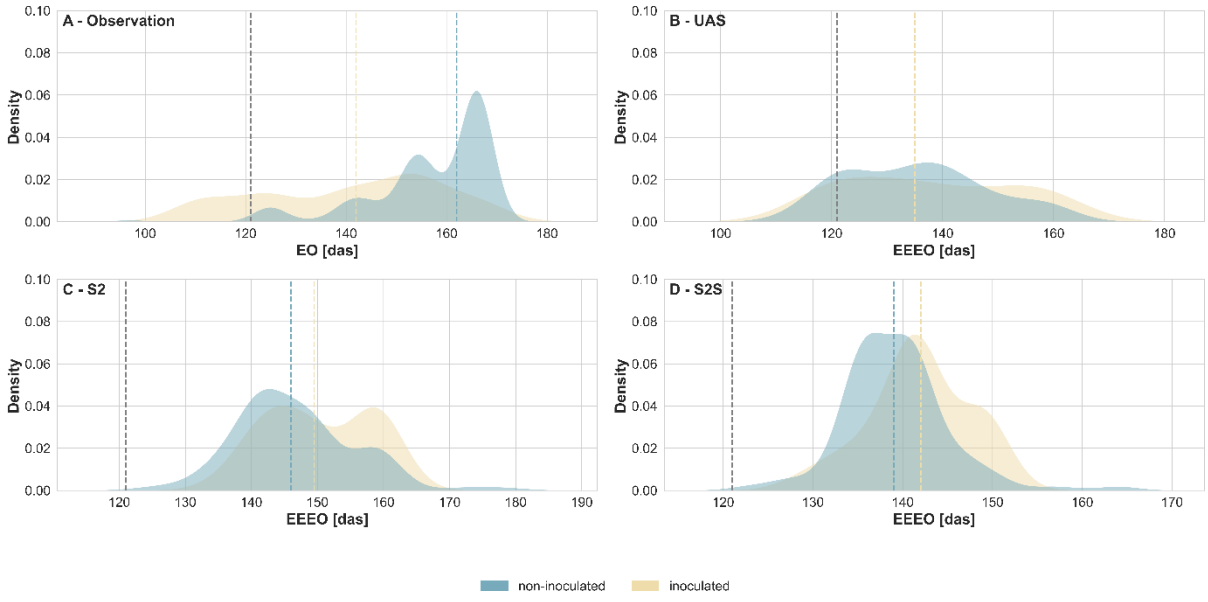


520

521 ***Figure 4.*** *The experimental site captured close to the median observed epidemic onset (A, 2022-09-03). Inoculation*
522 *sites are now clearly visible as circular bare patches. The observed epidemic onset (EO) dates (B) clearly show a*
523 *difference between inoculated and non-inoculated area. Visually, these differences are not obvious in the UAS*
524 *predicted (C), S2 predicted (D), and S2S predicted EEEO maps. The EEEO was predicted using the negative*
525 *prognosis model implemented in the cercospoRa package. Dark orange colors indicate later EO expressed in days*
526 *after sowing (das).*

527

528



529

530 ***Figure 5.*** *Observed epidemic onset (EO) and earliest estimated epidemic onset (EEEO) dates for Sentinel-2 (S2),*
531 *Sentinel-2 super-resolution (S2S), and UAS remote sensing data EO dates (A) – the time when at least 50% of*

plants at each assessment location showed CLS symptoms – was generated from within-field observations and expanded to the pixel scale with a vision transformer model. The observed canopy closure date (2022-07-30, 121 das, grey dashed line) and the median EO and EEEO dates have been added for the non-inoculated area (soft blue dashed line) and the inoculated area (linen white dashed line). S2, S2S, and UAS EEEO dates (B, C, D) were estimated using the cercospoRa negative prognosis model.

The General Additive Model (GAM) analysis indicated that the EEEO in non-inoculated areas occurs significantly earlier using the remote sensing data compared to the observed EO data (Table 6). Mean EEEO for Sentinel-2 was 10.3 days; Sentinel-2 super-resolution, 17.8 days; and UAS data resulted in the earliest EEEO on average by 21.7 days.

In the inoculated area, the GAM estimates show that the observed EO was approximately 15.9 days later than the non-inoculated areas. EEEO predicted by Sentinel-2 data in the inoculated area was approximately 19.9 days later than the observed EO in the inoculated area. S2S and UAS data showed a similar trend in the inoculated areas, both were significantly later than observed EO by a mean 19.1 and 18.8 days, respectively.

These results infer that the remote sensing data, particularly UAS, are effective in performing negative prognosis of the epidemic onset, however areas with an inoculation treatment has a significant impact on the timing of canopy closure which then affected epidemic onset. This was further confirmed by assessing the proportional success of EEEO values being earlier compared to spatially proximal observed reference values. Success for the negative prognosis model is defined by a EEEO date occurring prior to the visually confirmed EO date. All remote sensing data sources resulted in a greater proportional success in non-inoculated areas compared to the inoculated areas (Table 7).

TABLE 6 HERE

TABLE 7 HERE

Discussion

The episensing approach provide a relevant stop towards, mechanistically combining remote sensing observations with epidemiological modelling for greater automation of decision support systems. The R package *cercospoRa* developed for this study is available online (https://cran.r-project.org/web/packages/cercospoRa/index.html). We can show that the classic implementation of the CLS model by Wolf and Verreet (2005) through the *cercospoRa* package (Melloy et al. 2025) using remote sensing platforms such as S2, S2S and UAS were successful when estimating negative CLS prognosis at the field level in non-inoculated areas of the field trial which were subject infection from natural sources.

Furthermore airborne (UAS) and spaceborne (Sentinel-2, S2) remote sensing data aids in understanding within-field heterogeneity of earliest estimated epidemic onset (EEEO) to inform decision makers to areas where CLS is likely a higher risk compared to other areas. Especially high-resolution UAS data led to pixel-wise EEEO values that were markedly earlier (21 days) than the observed reference data.

For studying spatial patterns from remote sensing data, more information is needed on the effect of different disease intensities and their influence on canopy closure timing. In this study inoculum pressure caused the largest amount of variation negatively effecting successful CLS EEEO dates.

To our knowledge, we present a novel concept on a mechanistic combination of remote sensing derived structural plant parameters (leaf area index as a proxy for canopy closure) and epidemiological modelling, showing the advantages and general possibility to automate negative disease prognosis for crop protection.

Spatial Correlation Between Observed and Predicted Data?

While tempting to correlate the estimated onset dates from the *cercospoRa* negative prognosis model to observed onset dates, such an analysis, inherently, would not be informative. Successful EEEO dates from negative prognosis models occur any time prior to the actual onset, with model accuracy being associated with EEEO dates closer to EO. In this study spatially associating EEEO date pixels with proximal observed EO assessments at the sub-field level showed higher resolution UAS and S2S platforms provided greater success, 89 % and 85 % respectively in non-inoculated areas, compared to 75% success for the lower resolution S2. Inoculated areas showed much lower success with 52%, 56% and 46% of pixels returning EEEO dates before observed EO dates, for UAS, S2S and S2 respectively (Table 7). Inoculated areas trended towards later epidemic onset dates (Figure 5), which is not expected and explains the lower rates of success. Later EEEO in the inoculated areas was attributed to lower mean LAI values which were detectable as early as late June (Table 2). For the *cercospoRa* model, lower LAI corresponds to later canopy closure, which in turn leads to a later EEEO.

Inoculated areas could be interpreted as what might happen under high inoculum pressure and here remote sensing methods, while able to detect delayed canopy closure prior to observable CLS symptoms, produced later EEEO in the inoculated zone compared with visual EO confirmation. Thus, heavily infected fields might not be suitable for using this episensing approach without accounting for the additional inoculum pressure. Even though the UAS platform produced a mean EEEO date 2-3 days earlier than the EO date, caution should be exercised, and infield spatial heterogeneity might need to be compared to known spatial heterogeneity due to soil constraints. Also timing of infection, thus having knowledge on the origin of the

epidemic, is a variable that must be studied. Here, inoculated areas were inoculated earlier in plant development than non-inoculated areas. Thus, the pathogen had to move into the non-inoculated area and showed a phenotypic effect later compared to the inoculated areas. Further studies aim at testing the presented approach in natural infections. But this will require a careful selection of study sites considering landscape patterns and cropping history in the study area.

Additionally, the standard error in the Generalized Additive Model (GAM) for the inoculated plots is twice that of the non-inoculated plots for both EO and EEEO. This is likely due to a smaller sampling area and therefore sample size in the inoculated zone. Therefore, the smaller difference between EO and EEEO observed in the inoculated case is associated with a higher chance of unsuccessful model estimations, resulting in proportionally lower predictive success. Building on that issue, it was observed that the standard deviation is higher in UAS-derived EEEO compared to S2 and S2S, both having larger pixel sizes. Apart from the choice of study area and investigating the *cercospoRa* model on sites with natural infections only, the effect of spatial resolution on negative prognosis values should be studied as it also links back into the reference data.

Issues Obtaining Spatially Explicit Reference Data

For a reliable accuracy assessment, spatially explicit reference data is needed that captures spatial patterns at the appropriate scale. The classic workflow to assess the accuracy of remotely sensed data, not only in plant disease detection, is performed by comparing raster data values at specific positions with ground reference observations at the same position (Congalton 1991).

Developing models that predict the onset of plant disease epidemics at the pixel level using remote sensing data presents a significant challenge, particularly in obtaining

suitable reference data to test and validate model predictions. The core difficulty lies in the spatial and temporal precision required for reference data to align with the resolution and timing of remote sensing imagery.

The sugar beet trial we have been using to obtain reference data was sampled with great care, surveying more than 200 geospatially distributed field locations. Using these assessments when comparing the vegetation spatial heterogeneity (Figure 4A) with EO (Fig. 4B) and EEEO (Fig. 4 C-E) shows that spatial patterns are not picked up equally across different spatial resolutions from a remote sensing perspective. But also from a pathosystem perspective it is known that incidence and heterogeneity of incidence of plant diseases can vary between scales in a patch hierarchy (Turechek and Madden 2001).

While accuracy assessments can be quite simple, by comparing diseased host area with the associated pixel area (Bock et al. 2020), the demand for precise, georeferenced, and spatially dense field observations grows exponentially as spatial resolution increases. For example, at our UAS spatial resolution (i.e. 9.5 mm) it would have been necessary to modify the rating scale for it to cover areas below the area of a single leaf.

Coarser-resolution imagery such as Sentinel-2 (10 m), might be a more feasible pixel resolution to reference disease severity meaningful to decision makers, such as farmers and agronomists. Larger pixels, however, may dilute disease symptoms and canopy structure spatial heterogeneity showing highly uniform distributions between pixels, as can be seen in the spatial heterogeneity maps of the observed data (Figure 4B). This creates a scale-dependence problem: the patterns and variability observed at one resolution may not be visible—or may appear differently—at another. Moreover, aggregating or downscaling data can introduce distortion or mask localized anomalies,

661 leading to misinterpretation (Woodcock and Strahler 1987). These challenges are
662 especially important when studying dynamic or heterogeneous phenomena such as
663 disease outbreaks, where early indicators may be spatially subtle and easily lost at
664 coarser scales. However, applying remote sensing at different spatial resolutions
665 remains an existing endeavour to explore epidemic onset spatial variability.

666 Beyond the field-scale, similar shifts in epidemic onset for leaf rust (*Puccinia triticina*)
667 have been described (Caubel et al. 2017). Based on past, present, and future climate
668 scenarios, along with three different CO_2 emission scenarios in central Europe, it was
669 shown that the date when wheat rust severity reaches 5% can vary between 12 and
670 23 days. These results are attributed to the thermal conditions suitable for pathogen
671 development between crop emergence and the early phenological stage. Changing
672 temperatures under the predicted climate scenarios in Europe and elsewhere (Balting
673 et al. 2021; Naumann et al. 2021) will significantly affect the microclimate within the
674 canopy, especially during winter. Warmer winter temperatures create more favourable
675 conditions for fungal infection and development by shortening latency period leading
676 to more infection cycles. This, in combination with the findings presented here,
677 underscore the need to account for spatial variations in disease patterns to determine
678 the threshold for crop management actions across scales. Adoption of targeted
679 fungicide applications for disease hotspots is not wide-spread, and considering most
680 fungicide modes of action are more efficacious as protective sprays, rather than
681 curative, field-level fungicide applications are likely to remain common place. However,
682 the proposed negative prognosis approach can help growers manage CLS and
683 account for spatial heterogeneity by predicting periods when disease onset is highly
684 unlikely in a spatially explicit manner. This reduces unnecessary scouting and labor by
685 indicating when disease is not expected. It also prevents premature or unnecessary
686 fungicide applications, supporting cost savings and more sustainable crop protection.

By highlighting the periods and specific locations where disease risk becomes significant, the approach ensures that monitoring and interventions are timely and effective.

Still, the possibility to apply spatially explicit disease models present a number of challenges as described by Cunniffe (2015). While the suggestions to include factors such as introduction pathways, pathogen dispersal patterns, cryptic periods, landscape connectivity, and different detection technologies were made with invasive pathogens in mind, identical concepts apply at the field level and within-field. As shown with our methods to estimate canopy closure from LAI, the direction future studies should account for the spatiotemporal lag in negative prognosis models by using spatiotemporal variograms (Hurley and Leslie 2024) or lagged regression models (Kuiper and Ryan 2020).

Tracking Spatial Heterogeneity

Factors such as climate, topography, and human activity cause substantial variation in vegetation and soil traits across spatial and temporal scales (Garrigues et al. 2008; Gebbers and Adamchuk 2010; Pätzold et al. 2020; Stafford 2000). The LAI is a critical parameter in crop production and natural vegetation studies, as it directly relates to photosynthetic capacity, transpiration, and energy absorption, serving as a key indicator of plant health and productivity (Fang et al. 2019; Gebbers et al. 2011). LAI is particularly valuable in precision agriculture, where understanding within-field soil variability and its spatially explicit effects on crops is essential for optimizing nutrient management and disease control (Gebbers et al. 2011; Haboudane et al. 2004; Moulin et al. 1998). In this study, the field exhibited a non-homogeneous pattern characterized by variations in canopy density and varying-sized areas of exposed soil, which affected the timing and estimation of canopy closure (Figure 1 & 4). We accounted for this

712 spatial variation in the generalized additive model (GAM) analysis by applying a spline
713 to the spatial coordinates of observations (Fig. S6). However, such an approach
714 requires caution, as overfitting the response to sampling locations' spatial coordinates
715 may obscure actual disease effects. Given the inherent variability and error sources
716 posed by the pathosystem and environment, minimizing methodological errors is
717 particularly beneficial.

718 A key methodological criticism in this study is the use of turbid-medium radiative
719 transfer models (RTMs) for estimating plant traits in row crops. These models were
720 primarily designed for homogeneous canopies and are theoretically less suited for
721 discontinuous, non-uniform row crops (Jacquemoud et al. 2000; Jay et al. 2017;
722 Richter et al. 2011). Nonetheless, studies have achieved reasonable estimations of
723 leaf and canopy chlorophyll content and LAI in row crops using RTMs, including
724 applications in sugar beet trials (Andrieu et al. 1997; Dorigo 2012; Duan et al. 2014;
725 Jay et al. 2017). Successful RTM application in row crops is feasible during later
726 phenotypic stages when fractional vegetation cover is high and leaf clumping and
727 canopy heterogeneity are minimized (Han et al. 2023; Jay et al. 2017). Additionally,
728 aligning pixel size with row gaps ensures that each pixel captures a relatively
729 homogeneous canopy, optimizing trait retrieval (Jay et al. 2017) In our study, a dry
730 season led to patchy vegetation cover in many field sections. At high spatial resolutions
731 (e.g., UAS imagery), pixels retain less soil spectral interference compared to coarser
732 satellite imagery. While RTMs are increasingly optimized for row crops (Hu et al. 2024;
733 Ma et al. 2020), alternative approaches like empirical canopy cover estimation using
734 spectral vegetation indices (Haboudane et al. 2004) could also be tested to reduce
735 methodological uncertainty.

A second source of uncertainty lies in selecting the most appropriate LAI value for determining canopy closure timing. The data in this study were derived from a sugar beet trial affected by prolonged drought, which may have altered both the timing of canopy closure, and the associated LAI compared to typical growing conditions. Such year-to-year variability in LAI at equivalent growth stages has been documented in barley genotypes, where environmental factors (e.g., nitrogen availability, climate) outweighed genetic and management influences (Nowak et al. 2024).

Tillier et al. (2023) recently examined relationships between sugar beet yield, light interception, and canopy architecture, measuring LAI in four varieties with distinct leaf angle types (erectophile, planophile, and two intermediates). The erectophile type exhibited slower canopy closure and a lower effective LAI (Fang et al. 2019) at 90% canopy cover (LAI ≈ 2) compared to planophile varieties, as steeper leaf angles delay horizontal row coverage and reduce light interception efficiency.

Further supporting this variability, Hoffmann and Blomberg (2004) used NDVI from aerial imagery to model LAI across six management regimes, finding significant differences in LAI between years and seasons. For example, June LAI values ranged from 2–3 in 2001 but dropped to ~1 in 2002, highlighting the critical role of environmental conditions in LAI dynamics.

Hoffmann (2019) describes that LAI closely follows thermal time, can exceed 4.5, and declines after approximately 1300 growing degree days, remaining above an optimum value of 3.5. Under biotic stress from CLS, new leaf flush can be observed in later stages of disease progression, consequently influencing LAI development (Baryga et al. 2025). While the timing of reaching this optimum LAI varies among treatments, varieties, and years, differences in LAI between years and varieties during a growing season are generally stable. Hoffmann (2019) concludes that high-yielding years lead

to earlier canopy closure and consistently greater canopy cover. The studies outlined above indicate that leaf area formation is influenced by various factors but generally follows a sigmoidal development before declining, either through biotic stress or natural senescence, in late summer, as observed by Günder et al. (2022). Consequently, this sigmoidal LAI pattern is used in our methodology to model canopy closure based on LAI maps during the pre-symptomatic phase of CLS (i.e., early season, prior to exponential LAI development). To generate such LAI maps, researchers can combine remote sensing (e.g., UAV or satellite multispectral imagery) with radiative transfer models or vegetation indices, validated against reference measurements such as ceptometry or destructive sampling (Fang et al. 2019).

How to improve cercospoRa and apply it in practical agriculture?

To control CLS, the threshold system (Schwellenwertsystem) for fungicide application in sugar beet is a cornerstone of integrated pest management in Europe, particularly in Germany (Liebe et al. 2023). These thresholds are designed to ensure fungicides are only applied when economically justified, balancing effective disease control with minimal chemical input. This approach is often supported by weather-driven models (e.g., the CERCBET series) and regular field monitoring.

Several models, including the well-known CERCBET series, are currently used in CLS management, serving two interconnected purposes: predicting thresholds for fungicide application timing and guiding the leaf sampling (Blattrupfmethode) to monitor DI. The CERCBET series includes several models tailored to different needs:

- CERCBET 1 is a simple, regression-based model that predicts the regional first occurrence and spread of *C. beticola*. It supports the timing of field monitoring and has been validated and widely adopted in advisory practice.

- CERCBET 2 is a more complex, deterministic simulation model that uses detailed weather and crop data to simulate disease progress at the field level. Due to its complexity and sensitivity to initial conditions, it is primarily used for scientific research.

- CERCBET 3 is a weather-driven model derived from CERCBET 2, calculating daily infection pressure to assess epidemic risk and forecast when fungicide action thresholds may be exceeded. It is under ongoing development for field-specific decision support (Racca and Jörg 2003, 2007).

- CERCBET3 PLUS is the latest extension, introducing yield-based thresholds and recommending fungicide applications when predicted sugar yield losses reach 1%, thereby enabling more economically targeted interventions (ZEPP 2025).

Other forecasting systems for CLS include the Italian CERCOESY expert system, which influenced the development of the German CERCBET models, and BEETcast, used in North America (Battilani et al. 1997; Tedford et al. 2019). Most traditional models rely on weather data alone, but a recent approach by Hernandez et al. (2025) integrates early-season spore monitoring with weather criteria to trigger fungicide applications. By using spore abundance thresholds alongside refined weather conditions, this model reduced fungicide use without compromising disease control or yield, highlighting the benefits of incorporating biological monitoring into decision support systems.

Current CLS forecasting systems (e.g., CERCBET, BEETcast) rely heavily on weather and field history but overlook parameters such as explicit spore dynamics. Integrating spore dispersal kernels—mathematical models that quantify spatial spore distribution from inoculum sources—could enhance risk prediction by accounting for both local and neighbouring field inoculum. These kernels, informed by wind, rainfall, and landscape

data, would enable site-specific risk assessments and earlier interventions. Combining such models with spore monitoring (e.g., sentinel beets, Burkard traps) aligns with recent calls for biologically informed forecasting (El Jarroudi et al. 2020, 2021; Tedford et al. 2019). This approach would complement existing systems by addressing a critical gap: the spatial reality of pathogen spread. But also other approaches to model CLS seem appropriate. Skelsey (2021) demonstrated that anomaly detection algorithms can accurately forecast crop disease risk using only outbreak data, with a multimodel ensemble achieving higher accuracy and fewer alerts than existing national warning systems for potato late blight in Great Britain. This approach enabled flexible, region-specific disease forecasting and would be applicable to the presented pathosystem.

Outlook/Conclusion

Our work advances CLS modeling by introducing *cercospoRa*, an open-source R package that pre-epidemic negative prognosis at the pixel level using LAI products from Sentinel-2 and UAS. This FAIR-compliant tool addresses reproducibility challenges in plant pathology (Grünwald et al. 2024; Sparks et al. 2023) while capturing spatial heterogeneity in canopy closure—a critical factor masked by traditional field- or regional-scale models like CERCBET. By integrating radiative transfer modeling, the approach allows precise targeting of scouting efforts, reducing labor and improving early infection threshold detection.

We further demonstrate how super-resolution algorithms enhance Sentinel-2 LAI maps, bridging the gap between satellite and UAS data to enable scalable, high-resolution risk assessments (Aybar et al. 2024). This framework aligns with calls for spatially explicit epidemiology (Cunniffe et al. 2015; Mahlein et al. 2024; Mikaberidze et al. 2025) and adapts flexibly to research or farm contexts, despite inherent LAI retrieval limitations. By merging mechanistic modeling, open science, and precision

agriculture, *cercospoRa* offers a transparent, scalable tool to advance CLS management in sugar beet.

Acknowledgments

We gratefully acknowledge the invaluable contributions of Weronika Gajda and Dirk Koops. Weronika Gajda's insights and support significantly enhanced the handling of the example data presented here. Thanks to Dirk Koops and the technical staff for managing the experimental trial and collecting part of the data. Thanks to Dr. Dennis Grunwald for his critical revision of the manuscript.

References

Akhtman, Y. 2025. S2DR3: Effective 10-Band 10x Single Image Super-Resolution for Sentinel-2. Medium. https://medium.com/@ya_71389/sentinel-2-deep-resolution-3-0-c71a601a2253 (accessed 23 May 2025).

Andrieu, B., Baret, F., Jacquemoud, S., Malthus, T., and Steven, M. 1997. Evaluation of an improved version of SAIL model for simulating bidirectional reflectance of sugar beet canopies. Remote Sens. Environ. 60:247-257. https://doi.org/10.1016/S0034-4257(96)00126-5.

Asner, G. P. 1998. Biophysical and Biochemical Sources of Variability in Canopy Reflectance. Remote Sens. Environ. 64:234-253. https://doi.org/10.1016/S0034-4257(98)00014-5.

Aybar, C., Montero, D., Contreras, J., Donike, S., Kalaitzis, F., and Gómez-Chova, L. 2024. SEN2NAIP: A large-scale dataset for Sentinel-2 Image Super-Resolution. Sci. Data 11:1389. https://doi.org/10.1038/s41597-024-04214-y.

Balting, D. F., AghaKouchak, A., Lohmann, G., and Ionita, M. 2021. Northern Hemisphere drought risk in a warming climate. npj Clim. Atmos. Sci. 4:1-13. https://doi.org/10.1038/s41612-021-00218-2.

Baryga, A., Rusinowski, S., Krzyżak, J. et al. Sugar management and photosynthesis of sugar beet after infection by Cercospora beticola. Sci Rep 15, 19444 (2025). https://doi.org/10.1038/s41598-025-03968-8

Barreto, A., Ispizua Yamati, F. R., Varrelmann, M., Paulus, S., and Mahlein, A.-K. 2023. Disease Incidence and Severity of Cercospora Leaf Spot in Sugar Beet Assessed by Multispectral Unmanned Aerial Images and Machine Learning. Plant Dis. 107:188-200. https://doi.org/10.1094/PDIS-12-21-2734-RE.

Battilani, P., Giosuè, S., Racca, P., and Rossi, V. 1997. A Decision Support System for Cercospora Leaf Spot on Sugarbeet. In: Diagnosis and Identification of Plant Pathogens: Proceedings of the 4th International Symposium of the European Foundation for Plant Pathology, September 9–12, 1996, Bonn, Germany, eds. H.-W. Dehne, G. Adam, M. Diekmann, J. Frahm, A. Mauler-Machnik, and P. van Halteren. Dordrecht: Springer Netherlands, pp. 275-279. https://doi.org/10.1007/978-94-009-0043-1_57.

Berger, K., Atzberger, C., Danner, M., Wocher, M., Mauser, W., and Hank, T. 2018. Model-Based Optimization of Spectral Sampling for the Retrieval of Crop Variables with the PROSAIL Model. Remote Sensing 10:2063. https://doi.org/10.3390/rs10122063.

Berger, K., Machwitz, M., Kycko, M., Kefauver, S. C., Van Wittenberghe, S., Gerhards, M., Verrelst, J., Atzberger, C., van der Tol, C., Damm, A., Rascher, U., Herrmann, I., Paz, V. S., Fahrner, S., Pieruschka, R., Prikaziuk, E., Buchaillot, Ma. L., Halabuk, A., Celesti, M., Koren, G., Gormus, E. T., Rossini, M., Foerster, M., Siegmann, B., Abdelbaki, A., Tagliabue, G., Hank, T., Darvishzadeh, R., Aasen, H., Garcia, M., Pôças, I., Bandopadhyay, S., Sulis, M., Tomelleri, E., Rozenstein, O., Filchev, L., Stancile, G., and Schlerf, M. 2022. Multi-sensor spectral synergies for crop stress detection and monitoring in the optical domain: A review. Remote Sensing of Environment 280:113198. https://doi.org/10.1016/j.rse.2022.113198.

Bock, C. H., Barbedo, J. G. A., Del Ponte, E. M., Bohnenkamp, D., and Mahlein, A.-K. 2020. From visual estimates to fully automated sensor-based measurements of plant disease severity: status and challenges for improving accuracy. Phytopathol Res 2:9. https://doi.org/10.1186/s42483-020-00049-8.

Bundessortenamt. 2022. Beschreibende Sortenliste Getreide, Mais, Öl- und Faserpflanzen, Leguminosen, Rüben, Zwischenfrüchte. Bundessortenamt, Hannover, Germany. 300 pp.

Bundessortenamt. 2000. Richtlinien für die Durchführung von landwirtschaftlichen Wertprüfungen und Sortenversuchen. Landbuch Verlagsgesellschaft mbH, Hannover, Germany. 120 pp.

910 Caubel, J., Launay, M., Ripoche, D., Gouache, D., Buis, S., Huard, F., Huber, L., Brun,
911 F., and Bancal, M. O. 2017. Climate change effects on leaf rust of wheat: Implementing
912 a coupled crop-disease model in a French regional application. European Journal of
913 Agronomy 90:53–66. https://doi.org/10.1016/j.eja.2017.07.004.
914
915 CERCBET3+ - ZEPP. 2025. https://zepp.info/cercbet3/ (accessed 21 May 2025).
916 Chaloner, T. M., Fones, H. N., Varma, V., Bebber, D. P., and Gurr, S. J. 2019. A new
917 mechanistic model of weather-dependent Septoria tritici blotch disease risk. Phil.
918 Trans. R. Soc. B 374:20180266. https://doi.org/10.1098/rstb.2018.0266.
919
920 Congalton, R. G. 1991. A review of assessing the accuracy of classifications of
921 remotely sensed data. Remote Sensing of Environment 37:35–46.
922 https://doi.org/10.1016/0034-4257(91)90048-B.
923
924 Cunniffe, N. J., Koskella, B., E. Metcalf, C. J., Parnell, S., Gottwald, T. R., and Gilligan,
925 C. A. 2015. Thirteen challenges in modelling plant diseases. Epidemics 10:6–10.
926 https://doi.org/10.1016/j.epidem.2014.06.002.
927
928 Curran, P. J., and Milton, E. J. 1983. The relationships between the chlorophyll
929 concentration, LAI and reflectance of a simple vegetation canopy. International Journal
930 of Remote Sensing 4:247–255. https://doi.org/10.1080/01431168308948544.
931
932 Dorigo, W. A. 2012. Improving the Robustness of Cotton Status Characterisation by
933 Radiative Transfer Model Inversion of Multi-Angular CHRIS/PROBA Data. IEEE J. Sel.
934 Top. Appl. Earth Observations Remote Sensing 5:18–29.
935 https://doi.org/10.1109/JSTARS.2011.2171181.
936
937 Duan, S.-B., Li, Z.-L., Wu, H., Tang, B.-H., Ma, L., Zhao, E., and Li, C. 2014. Inversion
938 of the PROSAIL model to estimate leaf area index of maize, potato, and sunflower
939 fields from unmanned aerial vehicle hyperspectral data. International Journal of
940 Applied Earth Observation and Geoinformation 26:12–20.
941 https://doi.org/10.1016/j.jag.2013.05.007.
942
943 El Jarroudi, M., Chairi, F., Kouadio, L., Antoons, K., Sallah, A.-H. M., and Fettweis, X.
944 2021. Weather-Based Predictive Modeling of Cercospora beticola Infection Events in
945 Sugar Beet in Belgium. JoF 7:777. https://doi.org/10.3390/jof7090777.
946
947 El Jarroudi, M., Karjoun, H., Kouadio, L., and El Jarroudi, M. 2020. Mathematical
948 modelling of non-local spore dispersion of wind-borne pathogens causing fungal
949 diseases. Applied Mathematics and Computation 376:125107.
950 https://doi.org/10.1016/j.amc.2020.125107.
951
952 Eurostat. 2024. Agricultural production – crops. Statistics Explained. European
953 Commission. https://ec.europa.eu/eurostat/statistics-
954 explained/index.php?title=Agricultural_production_-_crops (accessed 28 May 2025).

Fang, H., Baret, F., Plummer, S., and Schaepman-Strub, G. 2019. An Overview of Global Leaf Area Index (LAI): Methods, Products, Validation, and Applications. Reviews of Geophysics 57:739–799. https://doi.org/10.1029/2018RG000608.

Fang, H., Liang, S., and Kuusk, A. 2003. Retrieving leaf area index using a genetic algorithm with a canopy radiative transfer model. Remote Sensing of Environment 85:257–270. https://doi.org/10.1016/S0034-4257(03)00005-1.

Faye, E., Rebaudo, F., Carpio, C., Herrera, M., and Dangles, O. 2017. Does heterogeneity in crop canopy microclimates matter for pests? Evidence from aerial high-resolution thermography. Agriculture, Ecosystems & Environment 246:124–133. https://doi.org/10.1016/j.agee.2017.05.027.

Feret, J.-B., François, C., Asner, G. P., Gitelson, A. A., Martin, R. E., Bidel, L. P. R., Ustin, S. L., le Maire, G., and Jacquemoud, S. 2008. PROSPECT-4 and 5: Advances in the leaf optical properties model separating photosynthetic pigments. Remote Sensing of Environment 112:3030–3043. https://doi.org/10.1016/j.rse.2008.02.012.

Garrett, K. A., Alcalá-Briseño, R. I., Andersen, K. F., Buddenhagen, C. E., Choudhury, R. A., Fulton, J. C., Hernandez Nopsa, J. F., Poudel, R., and Xing, Y. 2018. Network Analysis: A Systems Framework to Address Grand Challenges in Plant Pathology. Annu. Rev. Phytopathol. 56:559–580. https://doi.org/10.1146/annurev-phyto-080516-035326.

Garrigues, S., Allard, D., and Baret, F. 2008. Modeling temporal changes in surface spatial heterogeneity over an agricultural site. Remote Sensing of Environment 112:588–602. https://doi.org/10.1016/j.rse.2007.05.014.

Gebbers, R., and Adamchuk, V. I. 2010. Precision Agriculture and Food Security. Science 327:828–831. https://doi.org/10.1126/science.1183899.

Gebbers, R., Ehlert, D., and Adamek, R. 2011. Rapid Mapping of the Leaf Area Index in Agricultural Crops. Agronomy Journal 103:1532–1541. https://doi.org/10.2134/agronj2011.0201.

González-Domínguez, E., Caffi, T., Rossi, V., Salotti, I., and Fedele, G. 2023. Plant Disease Models and Forecasting: Changes in Principles and Applications over the Last 50 Years. Phytopathology® 113:678–693. https://doi.org/10.1094/PHYTO-10-22-0362-KD.

Grünwald, N. J., Bock, C. H., Chang, J. H., De Souza, A. A., Ponte, E. M. D., du Toit, L. J., Dorrance, A. E., Dung, J., Gent, D., Goss, E. M., Lowe-Power, T. M., Madden, L. V., Martin, F. N., McDowell, J., Naegele, R. P., Potnis, N., Quesada-Ocampo, L. M., Sundin, G. W., Thiessen, L., Vinatzer, B. A., and Zeng, Q. 2024. Open Access and Reproducibility in Plant Pathology Research: Guidelines and Best Practices.

Phytopathology® PHYTO-12-23-0483-IA. https://doi.org/10.1094/PHYTO-12-23-0483-IA.

Guan, J., and Nutter, F. W. 2002. Relationships between defoliation, leaf area index, canopy reflectance, and forage yield in the alfalfa-leaf spot pathosystem. Computers and Electronics in Agriculture 37:97–112. https://doi.org/10.1016/S0168-1699(02)00113-8.

Günder, M., Ispizua Yamati, F. R., Kierdorf, J., Roscher, R., Mahlein, A.-K., and Bauckhage, C. 2022. Agricultural plant cataloging and establishment of a data framework from UAV-based crop images by computer vision. GigaScience 11:giac054. https://doi.org/10.1093/gigascience/giac054.

Haboudane, D., Miller, J. R., Pattey, E., Zarco-Tejada, P. J., and Strachan, I. B. 2004. Hyperspectral vegetation indices and novel algorithms for predicting green LAI of crop canopies: Modeling and validation in the context of precision agriculture. Remote Sensing of Environment 90:337–352. https://doi.org/10.1016/j.rse.2003.12.013.

Han, D., Liu, J., Zhang, R., Liu, Z., Guo, T., Jiang, H., Wang, J., Zhao, H., Ren, S., and Yang, P. 2023. Evaluation of the SAIL Radiative Transfer Model for Simulating Canopy Reflectance of Row Crop Canopies. Remote Sensing 15:5433. https://doi.org/10.3390/rs15235433.

Heim, R., Wright, I., Scarth, P., Carnegie, A., Taylor, D., and Oldeland, J. 2019. Multispectral, Aerial Disease Detection for Myrtle Rust (Austropuccinia psidii) on a Lemon Myrtle Plantation. Drones 3:25. https://doi.org/10.3390/drones3010025.

Hernandez, A. P., Bloomingdale, C., Ruth, S., Cushnie, E., Trueman, C., Hanson, L., and Willbur, J. F. 2025. Early-season predictions of aerial spores to enhance infection model efficacy for Cercospora leaf spot management in sugarbeet. Plant Disease PDIS-10-24-2153-RE. https://doi.org/10.1094/PDIS-10-24-2153-RE.

Hoffmann, C. M. 2019. Importance of canopy closure and dry matter partitioning for yield formation of sugar beet varieties. Field Crops Research 236:75–84. https://doi.org/10.1016/j.fcr.2019.03.013.

Hoffmann, C. M., and Blomberg, M. 2004. Estimation of Leaf Area Index of Beta vulgaris L. Based on Optical Remote Sensing Data. Journal of Agronomy and Crop Science 190:197–204. https://doi.org/10.1111/j.1439-037X.2004.00093.x.

Homolová, L., Malenovský, Z., Clevers, J. G. P. W., García-Santos, G., and Schaepman, M. E. 2013. Review of optical-based remote sensing for plant trait mapping. Ecological Complexity 15:1–16. https://doi.org/10.1016/j.ecocom.2013.06.003.

Hu, P., Zheng, B., Chen, Q., Grunefeld, S., Choudhury, M. R., Fernandez, J., Potgieter, A., and Chapman, S. C. 2024. Estimating aboveground biomass dynamics of wheat at small spatial scale by integrating crop growth and radiative transfer models with satellite remote sensing data. Remote Sensing of Environment 311:114277. https://doi.org/10.1016/j.rse.2024.114277.

Hurley, B. J., and Leslie, T. F. 2024. Spatiotemporal Variograms as Neighborhood Definers. Geographical Analysis 56:404–424. https://doi.org/10.1111/gean.12382.

Imbusch, F., Liebe, S., Erven, T., and Varrelmann, M. 2021. Dynamics of cercospora leaf spot disease determined by aerial spore dispersal in artificially inoculated sugar beet fields. Plant Pathology 70:853–861. https://doi.org/10.1111/ppa.13337.

Jackson, R. D. 1986. Remote Sensing of Biotic and Abiotic Plant Stress. Annu. Rev. Phytopathol. 24:265–287. https://doi.org/10.1146/annurev.py.24.090186.001405.

Jacquemoud, S., Bacour, C., Poilvé, H., and Frangi, J.-P. 2000. Comparison of Four Radiative Transfer Models to Simulate Plant Canopies Reflectance: Direct and Inverse Mikaberidze, A., Cruz, C. D., Zerihun, A., Barreto, A., Beck, P., Calderón, R., Camino, C., Campbell, R. E., Delalieux, S. K. L., Fabre, F., Falla, E., Fraser, S., Gold, K. M., Gongora-Canul, C., Hamelin, F., Harteveld, D. O. C., Hong, C.-F., Leclerc, M., Lee, D.-Y., Lobo Jr., M., Mahlein, A.-K., McLay, E., Melloy, P., Parnell, S., Rascher, U., Rich, J., Salotti, I., Soubeyrand, S., Sprague, S., Surano, A., Takooree, S. D., Taylor, T. H., Touzeau, S., Zarco-Tejada, P. J., and Cunniffe, N. J. 2025. Opportunities and challenges in combining optical sensing and epidemiological modelling. Phytopathology 115:1169–1234. https://doi.org/10.1094/PHYTO-11-24-0359-FI.

Mode. Remote Sensing of Environment 74:471–481. https://doi.org/10.1016/S0034-4257(00)00139-5.

Jay, S., Maupas, F., Bendoula, R., and Gorretta, N. 2017. Retrieving LAI, chlorophyll and nitrogen contents in sugar beet crops from multi-angular optical remote sensing: Comparison of vegetation indices and PROSAIL inversion for field phenotyping. Field Crops Research 210:33–46. https://doi.org/10.1016/j.fcr.2017.05.005.

Jones, H. G., and Vaughan, R. A. 2010. *Remote sensing of vegetation: principles, techniques, and applications*. Oxford ; New York: Oxford University Press.

Khan, J., Del Río, L. E., Nelson, R., and Khan, M. F. R. 2007. Improving the Cercospora Leaf Spot Management Model for Sugar Beet in Minnesota and North Dakota. Plant Dis 91:1105–1108. https://doi.org/10.1094/PDIS-91-9-1105.

Kruse, F. A., Lefkoff, A. B., Boardman, J. W., Heidebrecht, K. B., Shapiro, A. T., Barloon, P. J., and Goetz, A. F. H. 1993. The spectral image processing system (SIPS)—interactive visualization and analysis of imaging spectrometer data. Remote Sensing of Environment 44:145–163. https://doi.org/10.1016/0034-4257(93)90013-N.

Kuiper, R. M., and and Ryan, O. 2020. Meta-analysis of Lagged Regression Models: A Continuous-time Approach. Structural Equation Modeling: A Multidisciplinary Journal 27:396–413. https://doi.org/10.1080/10705511.2019.1652613.

Kuska, M. T., Heim, R. H. J., Geedicke, I., Gold, K. M., Brugger, A., and Paulus, S. 2022. Digital plant pathology: a foundation and guide to modern agriculture. J Plant Dis Prot 129:457–468. https://doi.org/10.1007/s41348-022-00600-z.

Liebe, S., Imbusch, F., Erven, T., and Varrelmann, M. 2023. Timing of fungicide application against Cercospora leaf spot disease based on aerial spore dispersal of Cercospora beticola in sugar beet. Journal of Plant Diseases and Protection 130. https://doi.org/10.1007/s41348-023-00708-w.

Ma, X., Wang, T., and Lu, L. 2020. A Refined Four-Stream Radiative Transfer Model for Row-Planted Crops. Remote Sensing 12:1290. https://doi.org/10.3390/rs12081290.

Mahlein, A.-K., Arnal Barbedo, J. G., Chiang, K.-S., Del Ponte, E. M., and Bock, C. H. 2024. From Detection to Protection: The Role of Optical Sensors, Robots, and Artificial Intelligence in Modern Plant Disease Management. Phytopathology®. https://doi.org/10.1094/PHYTO-01-24-0009-PER.

Melloy, P., Heim, R., and Okole, N. 2024. cercospoRa: Process based epidemiological model for cercospora leaf spot of sugar beet. R package version 0.0.1. https://CRAN.R-project.org/package=cercospoRa

Lehnert, L. W., Meyer, H., Obermeier, W. A., Silva, B., Regeling, B., and Bendix, J. 2019. Hyperspectral Data Analysis in R : The hsdar Package. J. Stat. Soft. 89. https://doi.org/10.18637/jss.v089.i12.

Morris, C. E., Géniaux, G., Nédellec, C., Sauvion, N., and Soubeyrand, S. 2022. One Health concepts and challenges for surveillance, forecasting, and mitigation of plant disease beyond the traditional scope of crop production. Plant Pathology 71:86–97. https://doi.org/10.1111/ppa.13446.

Moulin, S., Bondeau, A., and Delecolle, R. 1998. Combining agricultural crop models and satellite observations: From field to regional scales. International Journal of Remote Sensing 19:1021–1036. https://doi.org/10.1080/014311698215586.

Naumann, G., Cammalleri, C., Mentaschi, L., and Feyen, L. 2021. Increased economic drought impacts in Europe with anthropogenic warming. Nat. Clim. Chang. 11:485–491. https://doi.org/10.1038/s41558-021-01044-3.

Nielsen, D. C., Miceli-Garcia, J. J., and Lyon, D. J. 2012. Canopy Cover and Leaf Area Index Relationships for Wheat, Triticale, and Corn. Agronomy Journal 104:1569–1573. https://doi.org/10.2134/agronj2012.0107n.

Nowak, R., Szczepanek, M., Błaszczyk, K., and Hassanpouraghdam, M. B. 2024. Response of photosynthetic efficiency parameters and leaf area index of alternative barley genotypes to increasing sowing density. Sci Rep 14:29779. https://doi.org/10.1038/s41598-024-81783-3.

Ojiambo, P. S., Yuen, J., Van Den Bosch, F., and Madden, L. V. 2017. Epidemiology: Past, Present, and Future Impacts on Understanding Disease Dynamics and Improving Plant Disease Management—A Summary of Focus Issue Articles. Phytopathology® 107:1092–1094. https://doi.org/10.1094/PHYTO-07-17-0248-FI.

Pätzold, S., Hbirkou, C., Dicke, D., Gerhards, R., and Welp, G. 2020. Linking weed patterns with soil properties: a long-term case study. Precision Agric 21:569–588. https://doi.org/10.1007/s11119-019-09682-6.

Pielaat, A., van den Bosch, F., Fitt, B. D. L., and Jeger, M. J. 2002. Simulation of vertical spread of plant diseases in a crop canopy by stem extension and splash dispersal. Ecological Modelling 151:195–212. https://doi.org/10.1016/S0304-3800(01)00484-7.

Racca, P., and Jörg, E. 2007. CERCBET 3 – a forecaster for epidemic development of Cercospora beticola*. EPPO Bulletin 37:344–349. https://doi.org/10.1111/j.1365-2338.2007.01136.x.

Racca, P., and Jörg, E. 2003. Prognose von Cercospora beticola mit den CERCBET-Modellen. Gesunde Pflanzen 55:62–69. https://doi.org/10.1046/j.1439-0345.2003.02093.x.

Rangel, L. I., Spanner, R. E., Ebert, M. K., Pethybridge, S. J., Stukenbrock, E. H., De Jonge, R., Secor, G. A., and Bolton, M. D. 2020. *Cercospora beticola* : The intoxicating lifestyle of the leaf spot pathogen of sugar beet. Molecular Plant Pathology 21:1020–1041. https://doi.org/10.1111/mpp.12962.

Richter, K., Atzberger, C., Vuolo, F., and D'Urso, G. 2011. Evaluation of Sentinel-2 Spectral Sampling for Radiative Transfer Model Based LAI Estimation of Wheat, Sugar Beet, and Maize. IEEE Journal of Selected Topics in Applied Earth Observations and Remote Sensing 4:458–464. https://doi.org/10.1109/JSTARS.2010.2091492.

Saiz-Rubio, V., and Rovira-Más, F. 2020. From Smart Farming towards Agriculture 5.0: A Review on Crop Data Management. Agronomy 10:207. https://doi.org/10.3390/agronomy10020207.

Savary, S., Willocquet, L., Pethybridge, S. J., Esker, P., McRoberts, N., and Nelson, A. 2019. The global burden of pathogens and pests on major food crops. Nat Ecol Evol 3:430–439. https://doi.org/10.1038/s41559-018-0793-y.

Schaepman-Strub, G., Schaepman, M. E., Painter, T. H., Dangel, S., and Martonchik, J. V. 2006. Reflectance quantities in optical remote sensing—definitions and case studies. Remote Sensing of Environment 103:27–42. https://doi.org/10.1016/j.rse.2006.03.002.

Shah, D. A., Paul, P. A., De Wolf, E. D., and Madden, L. V. 2019. Predicting plant disease epidemics from functionally represented weather series. Phil. Trans. R. Soc. B 374:20180273. https://doi.org/10.1098/rstb.2018.0273.

Shane, W., and Teng, P. 1992. Impact of Cercospora leaf spot on root weight, sugar yield, and purity of Beta vulgaris. Plant Disease 812–820.

Skelsey, P. 2021. Forecasting risk of crop disease with anomaly detection algorithms. Phytopathology, 111(2), 321-332. https://doi.org/10.1094/PHYTO-05-20-0185-R

Spanner, R., Neubauer, J., Heick, T. M., Grusak, M. A., Hamilton, O., Rivera-Varas, V., de Jonge, R., Pethybridge, S., Webb, K. M., Leubner-Metzger, G., Secor, G. A., and Bolton, M. D. 2022. Seedborne Cercospora beticola Can Initiate Cercospora Leaf Spot from Sugar Beet (Beta vulgaris) Fruit Tissue. Phytopathology® 112:1016–1028. https://doi.org/10.1094/PHYTO-03-21-0113-R.

Sparks, A. H., Ponte, E. M. D., Alves, K. S., Foster, Z. S. L., and Grünwald, N. J. 2023. Openness and Computational Reproducibility in Plant Pathology: Where We Stand and a Way Forward. Phytopathology® 113:1159–1170. https://doi.org/10.1094/PHYTO-10-21-0430-PER.

Stafford, J. V. 2000. Implementing Precision Agriculture in the 21st Century. Journal of Agricultural Engineering Research 76:267–275. https://doi.org/10.1006/jaer.2000.0577.

Tedford, S. L., Burlakoti ,Rishi R., Schaafsma ,Arthur W., and and Trueman, C. L. 2019. Optimizing management of cercospora leaf spot (Cercospora beticola) of sugarbeet in the wake of fungicide resistance. Canadian Journal of Plant Pathology 41:35–46. https://doi.org/10.1080/07060661.2018.1561518.

Tillier, L. C., Murchie, E. H., and Sparkes, D. L. 2023. Does canopy angle influence radiation use efficiency of sugar beet? Field Crops Research 293:108841. https://doi.org/10.1016/j.fcr.2023.108841.

Tittonell, P., Muriuki, A., Klapwijk, C. J., Shepherd, K. D., Coe, R., and Vanlauwe, B. 2013. Soil Heterogeneity and Soil Fertility Gradients in Smallholder Farms of the East

African Highlands. Soil Science Society of America Journal 77:525–538. https://doi.org/10.2136/sssaj2012.0250.

Turechek, W. W., and Madden, L. V. 2001. Effect of scale on plant disease incidence and heterogeneity in a spatial hierarchy. Ecological Modelling 144:77–95. https://doi.org/10.1016/S0304-3800(01)00350-7.

Ullrich, J., and Schrödter, H. 1966. Das Problem der Vorhersage des Auftretens der Kartoffelkrautfäule (Phytophthora infestans) und die Möglichkeit seiner Lösung durch eine „Negativprognose". Nachrichtenblatt des Deutschen Pflanzenschutzdienstes 18:33–40.

Vereijssen, J., Schneider, J. H. M., and Jeger, M. J. 2007. Epidemiology of Cercospora Leaf Spot on Sugar Beet: Modeling Disease Dynamics Within and Between Individual Plants. Phytopathology® 97:1550–1557. https://doi.org/10.1094/PHYTO-97-12-1550.

Verhoef, W., Jia, L., Xiao, Q., and Su, Z. 2007. Unified Optical-Thermal Four-Stream Radiative Transfer Theory for Homogeneous Vegetation Canopies. IEEE Trans. Geosci. Remote Sensing 45:1808–1822. https://doi.org/10.1109/TGRS.2007.895844.

Vidal, T., Lusley, P., Leconte, M., Vallavieille-Pope, C. de, Huber, L., and Saint-Jean, S. 2017. Cultivar architecture modulates spore dispersal by rain splash: A new perspective to reduce disease progression in cultivar mixtures. PLOS ONE 12:e0187788. https://doi.org/10.1371/journal.pone.0187788.

West, J. S., Bravo, C., Oberti, R., Lemaire, D., Moshou, D., and McCartney, H. A. 2003. The potential of optical canopy measurement for targeted control of field crop diseases. Annu. Rev. Phytopathol. 41:593-614. https://doi.org/10.1146/annurev.phyto.41.121702.103726.

Wolf, P. F. J., and Verreet, J. A. 2005. Factors affecting the onset of cercospora leaf spot epidemics in sugar beet and establishment of disease-monitoring thresholds. Phytopathology 95:269–274. https://doi.org/10.1094/PHYTO-95-0269.

Wood, S. N. 2017. *Generalized Additive Models: An Introduction with R, Second Edition*. 2nd ed. New York: Chapman and Hall/CRC. https://doi.org/10.1201/9781315370279.

Woodcock, C. E., and Strahler, A. H. 1987. The factor of scale in remote sensing. Remote Sensing of Environment 21:311–332. https://doi.org/10.1016/0034-4257(87)90015-0.

ZEPP. 2025. CERCBET3+ – Neue Bekämpfungsschwelle für Folgeapplikationen gegen Cercospora beticola in Zuckerrüben. ZEPP – Zentrale Einrichtung für Pflanzenschutz. Available at: https://zepp.info/cercbet3/. Accessed 16 June 2025.

Zou, X., Haikarainen, I., Haikarainen, I. P., Mäkelä, P., Mõttus, M., and Pellikka, P. 2018. Effects of Crop Leaf Angle on LAI-Sensitive Narrow-Band Vegetation Indices Derived from Imaging Spectroscopy. Applied Sciences 8:1435. https://doi.org/10.3390/app8091435.

Tables

Table 1. *List of structural and biochemical plant parameters that were used to invert the PRO4SAIL (PS = PROSPECT, 4S = 4SAIL) radiative transfer model for airborne and spaceborne remote sensing data. See footnote and supplementary material (S9) for abbreviations.*

	N	c_{ab}	c_{ar}	c_{br}	c_w	c_m	soil	lai	lidf	hspot	φ_{sun}	φ_{obs}	θ_{rel}
Min	1	20	8	0	0.03	0.009	0	0.1	1	0.01	10	0	180
Max	3.5	65	8	0	0.09	0.009	0	6.0	1	0.01	10	0	180
RTM	PS	PS	PS	PS	PS	PS	4S	4S	4S	4S	4S	4S	4S
Fixed	-	-	+	+	-	+	+	-	+	+	+	+	+

Table 2. *LAI descriptive statistics. Date column indicated the date of image acquisition.*

Area	Platform	Date	Count	Mean	SD	Min	25%	Median	75%	Max
Inoculated	S2	June 10	28	0.51	0.06	0.39	0.47	0.5	0.54	0.65
		June 30	28	0.51	0.06	0.39	0.47	0.5	0.54	0.65
	S2S	June 10	2523	0.58	0.11	0.32	0.5	0.57	0.65	0.86
		June 30	2523	0.58	0.11	0.32	0.5	0.57	0.65	0.86
	UAS	June 14	126	0.71	0.21	0.35	0.55	0.7	0.85	1.15
		June 28	116	0.72	0.14	0.35	0.6	0.75	0.85	1.05
Non-inoculated	S2	June 10	99	0.55	0.08	0.32	0.51	0.54	0.6	0.79
		June 30	99	0.55	0.08	0.32	0.51	0.54	0.6	0.79
	S2S	June 10	9416	0.61	0.11	0.24	0.54	0.62	0.69	0.99
		June 30	9416	0.61	0.11	0.24	0.54	0.62	0.69	0.99
	UAS	June 14	424	0.77	0.22	0.3	0.6	0.75	0.95	1.45
		June 28	397	0.74	0.13	0.45	0.65	0.75	0.8	1.2

Table 3. *Canopy closure summary statistics.*

Area	Platform	Count	Mean	SD	Min	25%	Median	75%	Max
Inoculated	S2	28	125.39	6.53	112	121	125	129.25	136
	S2S	26	117.97	5.83	105.08	114.33	119.08	122.58	126.08
	UAS	29	112.34	14.14	92	100	110	125	135
Non-Inoculated	S2	96	121.95	8.08	102	117	122	126	151
	S2S	99	115.03	6.21	99.08	111.08	114.08	119.08	141.08
	UAS	93	110.52	12.43	87	100	109	121	139

Table 4. *General Additive Model mean estimates of canopy closure in days after sowing (DAS) non-inoculated Sentinel-2 data (intercept). P values indicate statistical significance in comparison to the intercept.*

Variable	***Estimate***	***Std. Error***	***P value***
S2 (Intercept)	121.581	0.753	< 0.001
S2S	114.713	0.982	< 0.001
UAS	110.232	0.996	< 0.001
Inoculated Area	125.751	1.204	0.001

1286 ***Table 5.*** *Descriptive statistics for the observed (EO) and estimated earliest epidemic onset (EEEO).*

Area	Platform	Count	Mean	SD	Min	25%	Median	75%	Max
Inoculated	Observation (EO)	222	140.69	17.83	111	125	142	154	167
	S2 (EEEO)	28	150.32	7.8	136	142	149.5	158.25	160
	S2S (EEEO)	26	141.85	5.48	129	139.25	142	145.75	150
	UAS (EEEO)	29	137.86	14.86	117	123	135	149	160
Non-inoculated	Observation (EO)	791	157.02	12.14	97	153	162	166	167
	S2	96	146.62	8.85	125	141	146	150	178
	S2S	99	139.17	5.72	123	136	139	142	164
	UAS	93	135.31	12.5	113	123	135	142	162

1287

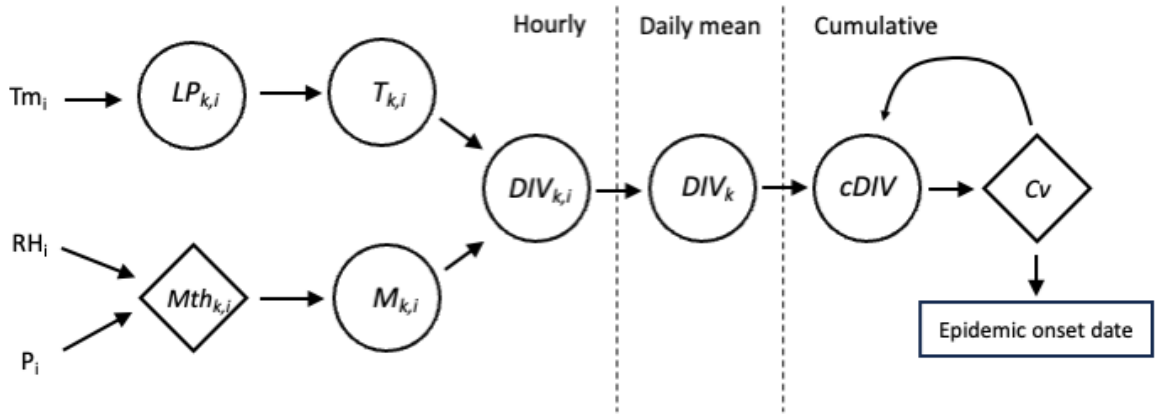
Table 6. *General Additive Model estimates of epidemic onset in days after sowing (das), Intercept represents non-inoculated observed epidemic onset (intercept). P values indicate statistical significance in comparison to the intercept.*

Variable	Estimate	Std. Error	P value
Observed: Non-Inoculated (Intercept)	156.940	0.439	< 0.001
S2	146.597	1.317	< 0.001
S2S	139.095	1.299	< 0.001
UAS	135.198	1.339	< 0.001
Observed: Inoculated Area	140.963	0.983	< 0.001
S2: Inoculated	150.587	2.775	< 0.001
S2S: Inoculated	142.244	2.839	< 0.001
UAS: Inoculated	138.347	2.753	< 0.001

Table 7. *Proportion success of estimated onset dates (EEEO) occurring prior to spatially proximal observed epidemic onset*

Platform	Area	n	∝ success
S2	non-inoculated	96	0.750
S2S	non-inoculated	99	0.848
UAS	non-inoculated	93	0.892
S2	inoculated	28	0.464
S2S	inoculated	26	0.577
UAS	inoculated	29	0.517

Supplementary Information



S1. Relational diagram of *cercospoRa* epidemiological model, adapted from Wolf and Verreet (2005). $Tm_{k,i}$ is the temperature at hour i in day $_K$; $RH_{k,i}$ is relative humidity; $P_{k,i}$ = rainfall; LP_i = temperature effect on the latent period; $T_{i,k}$ = temperature index or proportional progress towards the latent period; $DIV_{k,i}$ is the daily infection value calculated on hour *i* or the mean over 24 hours in the day *k;* cDIV is the cumulative daily infection values; Cv is the cultivar susceptibility threshold, circles indicate functions, diamonds, thresholds, input parameters have no shape.

S2. *cercospoRa function parameters. [1]When precipitation is provided, the model checks whether the precipitation of that day is higher than a given threshold, in which case RH is set to 100.*

Parameter	***Description***	***Unit***	***Value***
Tm	Temperature	Celsius [°C]	User Input
RH	Relative humidity	Percentage [%]	User Input
P	Rainfall (Optional)	Millimeter [mm]	User Input
Mth	Moisture threshold	70 % RH, 0.1 mm P	User Input
M	Moisture index	Proportion [no unit]	0 – 1
DIV	Daily infection value	Proportion [no unit]	0 – 1
cDIV	Cumulative daily infection values	Numeric [no unit]	0 – ∞
Cv	Cultivar resistance threshold, low values meet the threshold for epidemic sooner than genotypes with greater resistance	Numeric [no unit]	5, 7

S3 - calc DIV.R

C. beticola daily infection values (DIV) as described by Wolf and Verreet (2005), is based on hourly weather data and averaged over 24 hours (Eq.1 and Eq.2). Daily

infection values can range between zero (i.e., non-conducive disease development conditions) and one (i.e., ideal CLS development conditions leading to one whole infection cycle). Cumulative daily infection values (cDIV) can be interpreted as the number of infection cycles that have likely occurred. Threshold values for cDIV are thus the number of infection cycles allowed before intervention might be required to prevent yield-limiting disease levels. Thresholds could vary depending on cultivar susceptibility or pathogen aggressiveness which lead to slower disease development due to lower rates of infection success (lower infection rate) or lower fecundity (lower spore rate). Wolf and Verreet (2005) account for cultivar susceptibility by altering the cumulative DIV threshold, a lower threshold is applied to sugar beet genotypes with higher susceptibility (e.g. 3 for susceptible and 5 for tolerant). Daily infection values are computed from the product of temperature index (T_i) and moisture index (M_i).

$$cDIV = \sum_{k=1}^{n} DIV_k$$

Equation S1

where cDIV = cumulative daily infection value, k = kth day of record, and DIV_k = weather-dependent DIV for day k.

$$DIV_k = \frac{1}{24} * \sum_{k=1}^{24} T_{k,i} * M_{k,i}$$

Equation S1

where $T_{k,i}$ = temperature index in the hour (i) on the day (k) and $M_{k,i}$ = moisture index in the hour (*i*) on the day (*k*).

S4 -latent period.R

The effect of temperature is captured by the latent period (LP), which integrates the entire disease cycle period from inoculation, germination, infection, to symptom

appearance and production of new conidia (Wolf and Verreet 2005). The temperature index (T_i), is expressed as a ratio of $LP_{Tx,i}$ and LP_{opt}:

$$T_{k,i} = \frac{LP_{opt}}{LP_{Tx,i}}$$

Equation S2

where LP_{opt} = latent period at optimum temperature (here 21°C as default) and $LP_{Tx,i}$ = latent period at temperature T_{x_i} (°C) at hour *i*:

$$LP_{x,i} = 7 + 26 * e^{(0.35*(T_{x,i}-10))}$$

Equation S3

The moisture index (M_k, Eq. 6) includes information about precipitation and relative humidity. Calculation of M_k defines a humidity threshold (RH_{thresh}) below which no progress towards the latent period is made. The default threshold is defined as 90 % RH (RH_{user}).

$$RH_{thresh} = \frac{e^{\frac{140-RH_{user}}{21.7}}}{25}$$

Equation S4

The moisture index is then defined as:

$$M_{k,i} = \frac{1}{1 + e^{\frac{88-RH_{k,i}}{2.5*RH_{thresh}}}}$$

Equation S5

where $RH_{k,i}$ is the relative humidity for hour *i* on day *k*.

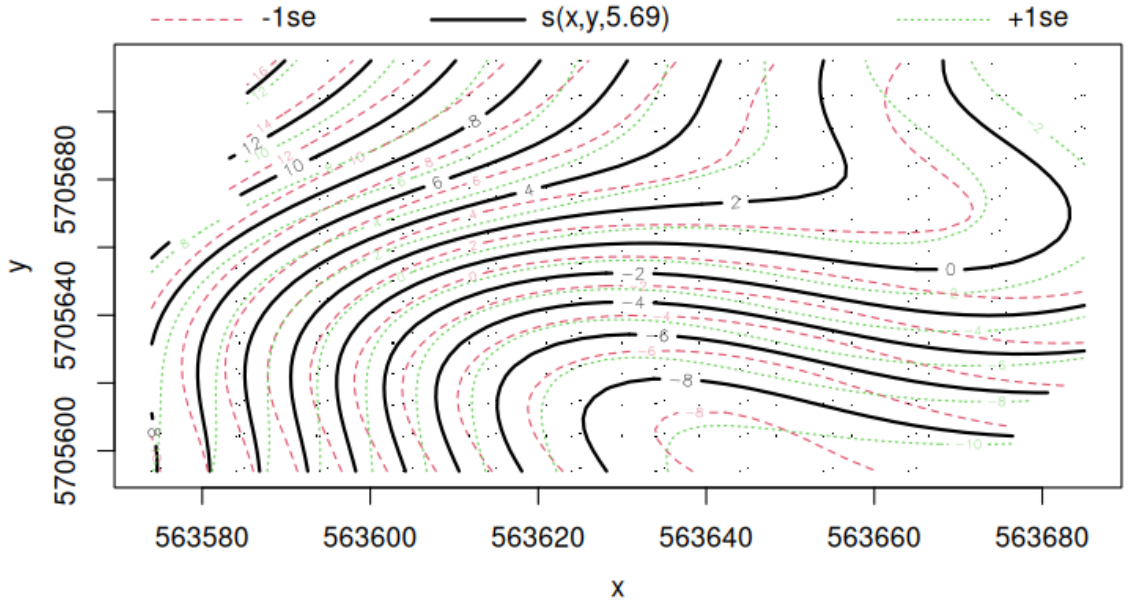
Also, a second option (Eq. 7) to calculate the latent period, using different function parameters has been implemented (El Jarroudi et al. 2021):

$$LP_{alt} = \frac{1}{0.00442 * T_{x,i} - 0.238}$$

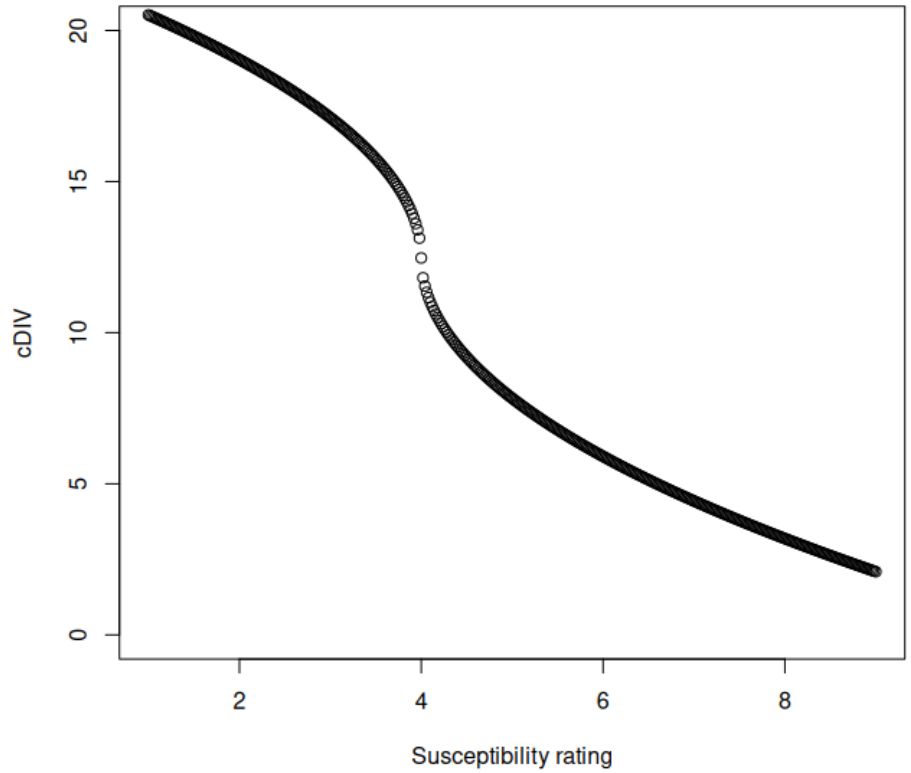
Equation S6

S5 -calc epidemic onset.R

The function calculates the timing of epidemic onset, defined as the time when 50% of the sugar beet plants had at least one lesion on one leaf. This stage of disease development is a very early stage and corresponds to an infected leaf area of about 0.01%. Instead of the first symptom appearance, this epidemic stage can be determined with high accuracy. The function allows to provide a date for canopy closure to start running the model.



S6. Spatial variation in canopy closure dates. Spatial patterns of canopy closure dates derived from the generalized additive model (GAM) analysis. Axes represent coordinates in the WGS 84 / UTM zone 32N (EPSG:32632) projected coordinate system (x: Easting [m], y: Northing [m]). Contour lines indicate the mean deviation (days) from the model intercept, illustrating localized delays or advancements in canopy closure relative to the field average.



S7 Daily Infection Values summed (cDIV) and mapped to the variety ranking system based on the published data in Wolf Verreet (2005).

S8 List of abbreviations used in the manuscript.

Abbreviation	Expansion	Dimension
C_{ab}	Chlorophyll a + b content	[ug*cm^{-2}]
C_{br}	brown pigment content	[unitless]
CC	Canopy closure	[g*cm^{-2}]
CLS	Cercospora leaf spot	n.a.
C_m	dry matter content	g*cm^{-2}
C_w	equivalent water thickness	[cm]
das	Days after sowing	[days after sowing]
EO	Epidemic onset	[days after sowing]
EEEO	Earliest estimated epidemic onset	[days after sowing]
GAM	General Additive Model	n.a.

hspot	hot spot parameter	[unitless]
LAI	Leaf area index	[m^2*m^{-2}]
lidf	leaf inclination distribution function	[unitless]
N	leaf structure parameter	[unitless]
RTM	Radiative transfer model	n.a.
SAM	Spectral angle mapper	n.a.
S2	Sentinel 2	n.a.
S2S	Sentinel 2 super-resolution	n.a.
φ_{obs}	observer zenith angle	[°]
soil	soil-brightness	[unitless]
φ_{sun}	sun zenith angle	[°]
θ_{rel}	relative azimuth angle	[°]
UAS	Uncrewed aerial system	n.a.